12-2006

Mathematical Modeling of High Temperature and High Pressure Dense Membrane for Separation of Hydrogen from Gasification

Ifeyinwa J. Iwuchukwu
University of Tennessee - Knoxville

To the Graduate Council:

I am submitting herewith a thesis written by Ifeyinwa J. Iwuchukwu entitled "Mathematical Modeling of High Temperature and High Pressure Dense Membrane for Separation of Hydrogen from Gasification." I have examined the final electronic copy of this thesis for form and content and recommend that it be accepted in partial fulfillment of the requirements for the degree of Master of Science, with a major in Chemical Engineering.

Atul C. Sheth, Major Professor

We have read this thesis and recommend its acceptance:

Roy Schulz, Narendra B. Dahotre

Accepted for the Council:
Carolyn R. Hodges

Vice Provost and Dean of the Graduate School

(Original signatures are on file with official student records.)

To the Graduate Council:

I am submitting herewith a thesis written by Ifeyinwa Jane Iwuchukwu entitled "Mathematical Modeling of High Temperature and High Pressure Dense Membrane for Separation of Hydrogen from Gasification." I have examined the final electronic copy of this thesis for form and content and recommend that it be accepted in partial fulfillment of the requirements for the degree of Master of Science, with a major in Chemical Engineering.

Atul C. Sheth

Major Professor

We have read this thesis

and recommend its acceptance:

Roy Schulz

Narendra B. Dahotre

Accepted for the Council:

Anne Mayhew

Vice Chancellor and Dean of Graduate Studies

(Original signatures are on file with official student records)

Mathematical Modeling of High Temperature and High Pressure Dense Membrane for Separation of Hydrogen from Gasification

A Thesis
Presented for the
Master of Science Degree
The University of Tennessee, Knoxville

Ifeyinwa Jane Iwuchukwu
December 2006

DEDICATION

This thesis is dedicated to my husband, Ernest Iwuchukwu, my daughter, Oge Iwuchukwu and my entire family whose faith and confidence in me never faltered.

ACKNOWLEDGMENT

I am deeply indebt to many people for their support and encouragement during my academic career at the UT Space institute. First of all, I would like to thank my major advisor, Dr. Atul C. Sheth for his patience, enthusiastic guidance, encouragement and helpful criticisms throughout the course of this work. Special thanks also go to Dr. Narendra B. Dahotre for his guidance and help throughout my work, and for serving as a member of the committee. I would also like to express my appreciation to Dr. Roy Schulz for his contributions and for serving as a member of the committee.

I commend the contributions of Dr. Garry Flandro, Dr. Kenneth Kimble, Dr. Magdalani, and Binay Singh, towards the success of this work.

To all my friends at UTSI, Patricia Bulks, Tina, Sricharan, Abraham, Sonya, Catherine, Rebecca, Mathew, Walter and Ashley, thank you for creating an enjoyable environment.

I am also indebted to my husband, Ernest and daughter, Oge. Too often they were without a wife and a mother, but they did so without a single complaint. I will also like to express my appreciation to my parents, Joseph Oranugo and Bridget Oranugo, for all their support.

Lastly, my profound gratitude goes to the Almighty God, my Creator and Sustainer for his guidance and inspiration throughout the course of this work.

ABSTRACT

There is an increasing interest in the use of inorganic membranes as a means of separating gas mixtures at high temperatures and pressures. The most important membrane properties are high permeability and selectivity, and good mechanical, thermal and chemical stability. Dense Pd-based composite membranes are suitable for hydrogen separation and use in catalytic membrane reactors because of their high permeability, good surface properties and high selectivity for hydrogen transport. At UTSI, Pd/Al_2O_3 membranes were prepared by a special method of laser based thermal deposition of the thin film Pd on a ceramic substrate by Nd-YAG laser irradiation of $PdCl_2$ coating on a γ-alumina substrate. This work reports a mechanistic model for the hydrogen permeation process in the Pd/Al_2O_3 composite membrane developed at UTSI. The model takes into account the well known kinetics of hydrogen adsorption/desorption in the palladium surface and hydrogen permeation in the porous alumina layer. Reasonable values for all mass transfer rate parameters were estimated based on the available surface science and membrane permeation literature. One set of experimental data (at 1100^0F) was used to determine the best values of the necessary rate parameters. These values of rate parameters were then used to predict and compare the experimental hydrogen flux data at two other temperatures (900^0F and 1300^0F). The results demonstrated that the atomic hydrogen diffusion through the palladium layer and pore diffusion in the porous alumina support both played important roles in the permeation of hydrogen through the composite Pd/Al_2O_3 membrane. A simplified resistance model was also employed to analyze the permeation behavior of hydrogen through the Pd/Al_2O_3 membrane to identify the major

resistances to the mass transfer. The results indicated that the mass transfer in the Pd layer contributed about 90% of the total mass transfer resistance. Our model calculations also indicated that by reducing the thickness of the Pd layer to about 18 μm, the DOE goal of > 60 scfh/ft^2 for hydrogen gas flux can be achieved. This can also be achieved by reducing the thickness of the Pd layer to about 20 μm and reducing the thickness of the alumina support layer to about 2 mm or by increasing it's porosity to about 50%.

TABLE OF CONTENTS

LIST OF TABLES

LIST OF FIGURES

LIST OF SYMBOLS

a	Lattice parameter (cm)
C	Gas phase molecular hydrogen concentration (mol/cm^3)
C_H	Hydrogen atom concentration (mol/cm^3)
C_i	Gas phase interface hydrogen concentration (mol/cm^3)
C_s	Gas phase molecular hydrogen concentration adjacent to surface (mol/cm^3)
C_1, C_2	Gas phase molecular hydrogen concentration on high and low partial pressure side of membrane, respectively (mol/cm^3)
D	Diffusion coefficient of hydrogen atoms in Pd (cm^2/s)
D_{H2}	Diffusion coefficient of hydrogen gas (cm^2/s)
D_e	Effective Knudsen diffusion coefficient in the porous alumina layer (cm^2/s)
D_K	Knudsen diffusion coefficient in the porous alumina layer (cm^2/s)
D_0	Pre-exponential factor for diffusion coefficient of hydrogen atoms in Pd, D (cm^2/s)
E_A	Activation energy for surface-to-bulk metal transition (kcal/mol H)
E_B	Activation energy for transition of H atom from bulk metal-to-surface (kcal/mol H)
E_d	Activation energy for H atom desorption (kcal/mol H)
E_{diff}	Activation energy for H atom diffusion in Pd (kcal/mol H)
ΔE_{ad}	Heat of adsorption (kcal/mol H_2)

ΔE_{ab}	Heat of absorption (dissolution) (kcal/mol H_2)
F_p	Gas permeability (mol /cm^2 s atm)
F_{pk}	Gas permeability due to Knudsen diffusion (mol /cm^2 s atm)
F_{pv}	Gas permeability due to viscous flow (mol /cm^2 s atm)
$\Delta \bar{G}_H$	Relative partial molar Gibb's free energy of dissolution for H in Pd (kcal/mol H)
h	Mass transfer coefficient (cm/s)
H_{ad}	Hydrogen atom in the bulk metal
H_{me}	Hydrogen atom in the chemisorbed site
$\Delta \bar{H}_H^0$	Relative partial molar enthalpy of dissolution at infinite dilution (kcal/mol H)
J	H_2 flux (mol/ cm^2 s)
J_H	H atom flux (mol/cm^2 s)
J_k	H_2 flux described by Knudsen's equation (mol/ cm^2 s)
J_v	H_2 flux described by Poisuielle's law (mol/ cm^2 s)
k	Boltzman constant (Joules/K)
k_o	Desorption rate constant pre-exponential factor (cm^2/mol Hs)
k_d''	Desorption rate constant based on N_{AA} (s^{-1})
k_d	Desorption rate constant (cm^2/mol H s)
K_s	Sievert's law constant ($atm^{0.5}$)
K_n	Knudsen number
L	Thickness of the porous support (cm)

M_{H2}	Molecular weight of H_2 (g/mol)
n	Pressure exponent (0.5-1)
N_{AA}	surface concentration of nearest neighbor occupied site pairs (mol pairs/cm^2)
N_b	Bulk metal Pd atom concentration (0.113 mol Pd /cm^3)
N_{av}	Avogadro's number (6.023×10^{23} molecules/g-mole)
N_{OA}	Surface concentration of nearest neighbor occupied/unoccupied site pairs (mol pairs/cm^2)
N_s	Pd atom surface concentration (mol Pd atoms/cm^2)
P_1, P_2	H_2 partial pressure on high and low partial pressure side of membrane, respectively (atm)
P_i	Interface pressure (atm)
P_m	Average pressure across the porous alumina support (atm)
R	Gas constant (cal/mole K)
R_{Pd}	Transport resistance in the dense Pd layer (m^2 s atm mol^{-1})
R_s	Transport resistance in the porous alumina support (m^2 s atm mol^{-1})
R_{tot}	Overall transport resistance (m^2 s atm mol^{-1})
S	Sticking coefficient (dimensionless)
S_0	Initial sticking coefficient (at zero coverage)
$\Delta\bar{S}_H^0$	Relative partial molar entropy of dissolution for hydrogen molecule at infinite dilution (kcal/ mol K)
t	Time (s)
T	Temperature (K)

$\overline{u}$	Mean molecular velocity (cm/s)
W	Pair-wise interaction energy between H atoms on surface (kcal/mol)
x_{H2}	Mole fraction of hydrogen in the gas mixture
x_i	Mole fraction of the other gas components in the gas mixture
X	Fraction of hydrogen atoms to Pd atoms (H/Pd ratio) in the bulk metal
X_1, X_2	Fraction of hydrogen atoms to Pd atoms (H/Pd ratio) in the bulk metal adjacent to high and low pressure surfaces respectively
X_{1s}, X_{2s}	Fraction of hydrogen atoms to Pd atoms (H/Pd ratio) in the bulk metal immediately adjacent to high and low pressure surfaces respectively
z	number of nearest neighbors on the surface
Δz	Thickness of membrane (μm)

Greek

α	constant that relates location of interstitial position to diffusional jumps
β_d	Rate constant for H atom for metal to surface transition (cm^3/mol H s)
β_0	Pre-exponential factor for β_d (cm^3/mol H s)
δ	Film thickness (cm)
ε	Porosity of the porous medium
Γ	Molecular bombardment rate at surface (mol H_2/cm^2 s)
Γ_j	Diffusive jump frequency (s^{-1})
Γ_{j0}	Pre-exponential factor for Γ_j (s^{-1})

υ_d	Rate constant for H atom for surface-to-bulk metal transition (cm^3/mol H s)
υ_0	Pre-exponential factor for υ_d (cm^3/mol H s)
θ	Surface coverage (Fraction of hydrogen atoms to Pd atoms (H/Pd ratio) on surface)
θ_1, θ_2	Surface coverage (Fraction of hydrogen atoms to Pd atoms (H/Pd ratio) on surface) on the high and low partial pressure sides of the membrane, respetively
θ_{00}	Probability of having two adjacent unoccupied sites on surface
τ	Tortuosity factor of a porous medium
μ	Gas viscosity (atm s)
λ	Mean free path of gas molecules (cm)
*	Free adsorption site

LIST OF ABBREVIATIONS

atm	Atmosphere
A	Occupied site
AA	Adjacent occupied sites pair
CO	Carbon monoxide
CH_4	Methane
DOE	Department of Energy
FCC	Faced Center Cubic
GC	Gas chromatography
H	Hydrogen atom
H_2	Hydrogen molecule
kcal	Kilocalories
kJ	Kilojoules
mol	Gram-mole
n	Nano
Nd-YAG	Neodymium-Yttrium Aluminum Garnet
O	Unoccupied site
OO	adjacent unoccupied sites pair
OA	Unoccupied /occupied pair
Pa	Pascal
Pd	Palladium
scfh /ft^2	Standard cubic feet per hour per square feet.

μ	Micro
UTSI	University of Tennessee Space Institute
LEED	Leadership in Energy and Environmental Design

1. INTRODUCTION

1.1 Background

The extensive use of hydrogen in many industrial sectors such as petroleum refining, petrochemical, semi-conductor, industrial material processing and in power producing devices such as fuel cells, is expected to rise in the coming years. More so, the depletion of crude oil, natural gas and fossil fuel has led the US chemical industry to seriously consider hydrogen as one of the alternative clean energy carriers. Hydrogen is the most common element in the universe but is mostly found bonded in chemical compounds like water, biomass and fossil fuels. Chemical reactions are needed to break hydrogen bonds from these compounds and release hydrogen which has to be then recovered from the multi-component gas stream. Recovery of high purity hydrogen can be achieved by employing the membrane separation technology. The DOE goal is to research and develop low cost, highly efficient hydrogen technologies from diverse domestic and renewable sources. Substantial advantages can be gained from fossil-fuel gasification technology for the production of hydrogen and other useful gases by using membrane separation processes. The reactions involved in gasification are favored at high temperature and pressure and are also limited by thermodynamic equilibrium. The use of a membrane for separation provides the basis for improved methods of hydrogen recovery and also reduces cost associated with hydrogen production at elevated temperatures and pressures. Also, combining the chemical reaction and separation steps in a single process will eliminate limitations imposed by the process thermodynamics on

the yield of hydrogen. The US chemical industry is also faced with the significant technical challenge of developing hydrogen separation membranes that can withstand severe operating conditions of high temperature, high pressure, and dusty environments.

Dense palladium-based membranes have been used in recent years in the separation of hydrogen, and in catalytic membrane reactors and have been studied extensively due to their high permeability, good surface properties and high selectivity for hydrogen transport. Palladium was first identified as a highly hydrogen-permeable material in the 19^{th} century and it is used for high-performance hydrogen-separation applications today (1). It is necessary to reduce the thickness of the Pd film in order to improve permeation flux and to retain the high selectivity of palladium-based membranes. However, very thin membranes have low mechanical strength. To achieve good mechanical strength and also to enhance the permeation rate of hydrogen, the Pd-based surface film is usually deposited on a mechanically strong porous support. Palladium-based composite membranes have high hydrogen permeability, very high hydrogen selectivity, and good mechanical and thermal stabilities at high temperature. Shu et al and many other investigators have prepared Pd-based composite membranes by the electro-less plating technique on micro-porous glass, porous stainless steel, and anodic alumina support (2). Sputter-deposition (3), spray pyrolysis (4), and chemical vapor deposition (5) have also been used to deposit Pd-based films on the suitable porous support.

The Pd/Al_2O_3 membranes discussed and researched in the present work consist of a very thin, dense Pd skin layer on a porous Al_2O_3 support. The permeation of hydrogen through the dense palladium is a complex multi-step process, which involves reversible dissociative chemisorption of hydrogen on the membrane surface, reversible dissolution of surface atomic hydrogen in the bulk layers of the metal and the diffusion of hydrogen in the membrane (6). This type of solution-diffusion mechanism was first proposed by Thomas Graham in 1888. The overall rate of permeation may be limited by one particular step if it is the slowest step or a combination of several steps. For bulk diffusion of hydrogen as the rate limiting step, the permeation rate of hydrogen through the dense Pd-based film was found to be inversely proportional to the membrane thickness and was also proportional to the square root of the pressure difference. This behavior is called Sievert's law behavior (1). Deviations from Sievert's law behavior have been attributed to various factors including the surface processes, surface poisoning, and grain size and grain boundaries (7). Membrane materials with larger grain size and fewer grain boundaries have lower permeability (5) and hence affect Sievert's law behavior. In the past few years many investigators have reported flux values for thick Pd membranes that are consistent with the calculation for diffusion limited permeation. Significant discrepancies exist for membranes less than 10μm thick. Desorption limited fluxes have also been reported at very low temperature. Additionally, the permeation through the porous Al_2O_3 support can be described by a phenomenological equation (Darcy's Law) in which the hydrogen flux is proportional to the pressure gradient across the Al_2O_3 support (2).

$$J = F_P(P_h - P_l) \quad (1.1)$$

Where

F_P = permeability

P_h and P_l = partial pressures of gas in the high pressure and low pressure sides respectively.

Hydrogen gas transport through the porous support in terms of Knudsen diffusion and viscous flow has also been analyzed by Huang and Chen (8) using the dust-gas model.

At UTSI, Pd/Al_2O_3 membranes were prepared by a special method of laser based thermal deposition of the thin film Pd on a ceramic substrate by Nd-YAG laser irradiation of $PdCl_2$ coating on γ-alumina substrate (9). In this UTSI study, the parameters of the laser beam were optimized, and a new procedure to synthesize metal-ceramic composite membranes was developed. The Pd-ceramic composite membrane showed good mechanical and thermal stability with a hydrogen permeability flux of 0.061 (mol/m^2s) and activation energy of about 5.39 (kJ/mol) in a temperature range of 900-1300°F (9).

1.2 Scope of Present Work

In this study, a mechanistic model of the hydrogen permeation process in the Pd/Al_2O_3 composite membrane is reported. This model takes into account the well known kinetics of H_2 adsorption/desorption at the palladium surface and H_2 permeation in the porous

alumina layer. It also takes into account the mass transfer resistance associated with the viscous flow (Hagen-Poisuielle type) and Knudsen diffusion through the porous support. This mechanistic model was used to simulate the earlier hydrogen permeation experimental results obtained from the Pd/Al_2O_3 composite membrane at UTSI (9). Based on the results obtained from our model calculations, the optimal material and structure of a composite membrane for hydrogen separation can be effectively designed to achieve the fluxes in excess of 60 $scfh/ft^2$. This limit has been considered by DOE to be necessary for the commercial applications in hydrogen fueled fuel cells.

In comparison between the rigorous theory and direct experimentation for hydrogen permeation membranes, the mathematical model developed based on theoretical approach can offer a quick and less expensive route to acquire information necessary for membrane development and design. It can be used to determine the trade-offs in conflicting design requirements, to choose optimum operating conditions, and to see the effect of various parameters on membrane performance. Such a model could also provide a basis to extrapolate results from small scale units to a prototype or to demonstration scale plant. Also information derived from such a study could also provide the ability to tailor-make membrane properties for desired applications.

2. LITERATURE REVIEW

There are excellent reviews on the fundamental mechanisms of gas transport through palladium membranes and on modeling of gas separation in palladium membranes. Huang et al. (2) studied the hydrogen permeation behaviors through palladium composite membranes, to understand the influence of the mass transfer resistance of the Al_2O_3 support. The importance of the Pd film microstructure on the hydrogen permeation rates has been stressed by Ward and Dao (7). A model was developed by Henis and Tripodi (1981), whereby the transport properties of each membrane layer in the composite hollow fiber membrane can be isolated and their transport resistances studied (10). Shu et al. reviewed hydrogen permeation in pure palladium membranes, as well as the basic physico-chemical knowledge which would allow for future development (6). The energetic, kinetic and structural properties of hydrogen chemisorbed on a Pd (100) surface were studied by Behm et al. using thermal desorption, work function and LEED (Leadership in Energy and Environmental Design) measurements (11). More work on the fundamental surface science of hydrogen on palladium has also been reported by Conrad et al. in his work on the adsorption of hydrogen on palladium single crystal surfaces (12).

Membranes are permeable or semi-permeable barriers that permit selective mass transport between two phases and can be broadly classified into organic and inorganic membranes. Transport processes across the membrane take place as a result of a driving force, which is typically associated with a gradient of concentration, pressure,

temperature, electric potential, etc. Organic membranes are typically made from polymers and inorganic membranes are comprised of membranes that are made from metals, glass and ceramics. Inorganic membranes are chemically and thermally more stable than organic membranes at temperatures over 473K. They also have better mechanical strength and freedom from aging. The permeation and separation efficiency of inorganic membrane systems depend, to a large extent, on the microstructural features of the membrane and the architecture of membranes and membrane support combinations (13). The microstructural features include, pore shape and morphology, pore size (distribution) and tortuosity. The architecture of membranes and membrane support combinations describes the way the different parts of the membrane system or module are shaped and combined. Membranes are manufactured in a diverse range of geometries; they include flat, tubular, multi-tubular, hollow-fiber and spiral-wound membranes. According to their structure, inorganic membranes can be divided into porous inorganic membranes and dense inorganic membrane. Porous membrane with average pore diameters larger than 50 nm are classified as macro porous, those with average pore diameters in the intermediate range between 2 and 50 nm as mesoporous and those with average pore diameters smaller than 2 nm as microporous membranes (14).

Dense membranes are made from solid layers of metals like platinum, silver, niobium, zirconium, palladium and their alloys. Transport across dense membranes is described by the solution/diffusion mechanism. In this mechanism, the molecular specie is adsorbed on the surface and then dissolved in the bulk of the membrane, where transport occurs by atomic diffusion through the bulk. It then desorbs from the surface of the permeate side

of the membrane. Dense membranes can either be self-supporting (symmetric) or composed of a thin selective layer deposited on a porous support (asymmetric). Self-supporting dense membranes are relatively thick with high selectivity and high mechanical strength, but low fluxes. The flux is inversely dependent on the thickness of the membrane. Besides the low flux, thick Pd membranes are too expensive for economic use. Thin selective membrane layers deposited on porous supports improve permeation rates and have great impact on the cost of membranes. Recently, research efforts have been carried out on fabricating thinner membrane layers on porous supports. Chemical vapor deposition has been used to deposit palladium thin films on a ceramic support (5, 15, and 16). The chemical plating method has been successfully used by researchers to coat membrane films of thickness 4 – 6 μm (3, 17). Li et al. (4) have successfully coated 2 μm thin Pd/Ag alloy membranes using spray pyrolysis technique. Shu et al. have studied the physical properties of simultaneously deposited films of palladium and silver by Electroless plating (18). Sputter-deposition techniques have also been used to deposit thin films on porous support. At UTSI, a special method of laser-based deposition of the thin Pd film on a ceramic substrate by Nd-YAG laser irradiation of $PdCl_2$ coating on γ-alumina substrate has been successfully carried out (9).

The first observation of the permeability of hydrogen through transition metals was made by Deville and Troost (19), whose experiments were first carried out on iron and platinum (Deville and Troost, 1863; Deville, 1864). Thomas Graham carried out related measurement afterwards and observed that not only did palladium permit high throughputs of hydrogen, but that large volumes of hydrogen were absorbed in the

palladium metal. The hydrogen permeability of palladium increases with the temperature because the endothermic activation energy for diffusion dominates the exothermic adsorption of hydrogen on palladium (20). Palladium exhibits a high solubility of hydrogen when compared with other transition elements over a very wide range of temperatures and pressures of hydrogen. Palladium experiences an α —> β transition at temperatures below the critical temperature (568K) and pressures below 20 atm (1, 6, 19), depending on the hydrogen concentration in the metal. This phase transition leads to lattice expansion of about 10% which leads to lattice strain and physical distortion after a few cycles. This can be remedied by exposing palladium to hydrogen only at high temperatures above the critical temperature. The surface of pure palladium metal is poisoned when exposed to sulfur and chlorine and the presence of carbon monoxide may affect its chemical stability. It has been reported that a CO concentration of only 0.2% gives a gives a significant reduction in the hydrogen flux (48, 49). Removal of hydrogen sulfide up front from the multi-component gas stream will reduce poisoning of the Pd surface. In addition, alloying palladium with other elements improves its chemical stability. Examples of such alloys of Pd are Pd-Ag, Pd-Cu and Pd-Ru. Pd-Cu membrane is resistant to sulfur. Pd-Ag is the most commonly used alloy for hydrogen extraction, the hydrogen permeability increases with silver content (17). Alloying Palladium with other elements increases the mechanical strength of palladium membrane and the lattice is less influenced by hydrogen unlike pure palladium membrane that undergoes lattice expansion after certain cycles of α —> β transformation. In, for example, palladium–silver alloys, the lattice has already been expanded by the silver atoms, and the Pd-Ag lattice is less influenced by hydrogen and thus less brittle than the pure Pd lattice (56).

Palladium is characterized by face-centered cubic (FCC) structure, which has two interstitial, octahedral and tetrahedral sites, corresponding to the minima in the potential energy (21). Diffusion of hydrogen through the palladium is attributed to the "jumping" of hydrogen atoms through the octahedral interstitial sites of the face-centered cubic palladium lattice (22). The lattice-diffusional mode of mass transfer for hydrogen has given palladium metal an unmatched potential for use as hydrogen selective membranes for separation and purification. The diffusion coefficient of hydrogen in palladium has been determined by several investigators with remarkable consistency. The diffusion coefficient is given by following equation:

$$D = D_0 \exp(-E_{diff} / RT) \qquad (2.1)$$

Where

D_0 = Pre-exponential factor (cm^2/s),

E_{diff} = activation energy for H atom diffusion (kcal/mol H),

T = temperature (K), and

R = gas constant (kcal/mole K).

In some selected literature permeation data, reported values of the pre-exponential factor range from 2.3×10^{-3} - $4.5 \times 10^{-3} cm^2/s$ and activation energy of H atom diffusion varying between 21.7 – 24.1 kcal/mol H in the temperature range of -40 to 1000^0C (23 – 27).

There has been growing interest in the industrial application of Pd-based membranes for hydrogen production. This is because the catalytic ability of the membrane surface combined with the high hydrogen selective permeation would make it possible to separate hydrogen from a reversible reaction and thereby shift the reaction towards the

product side. Pd-based membranes have been used as hydrogen purifiers to supply high purity hydrogen for industrial applications. A commercial hydrogen purification equipment utilizing tubes of 23% silver-palladium alloy was developed by Johnson Matthey in the early 1960's (6). Dehydrogenation and hydrogenation reactions on Pd membranes have been reviewed by Shu et al. (6). Gryaznov et al. studied the dehydrogenation of light alkane using Pd or Pd-alloy dense membranes (28) and Itoh (29) studied the dehydrogenation of cyclohexane in reactors using palladium tubes. Uemiya et al. (30) studied the water gas shift reaction using a palladium membrane reactor in which the product hydrogen permeated the membrane to provide CO conversions in excess of those associated with the normal equilibrium conversion.

Gas transport through palladium based membranes is usually rate limited by the bulk atomic diffusion and that the flux has been found to be inversely proportional to the membrane thickness with an approximate square root dependence on the hydrogen partial pressure (1, 2, 6 – 9). This behavior is called Sievert's law behavior with the value of the exponent, *n,* is equal to 0.5 (23). The exponent of 0.5 reflects the dissociation of the gaseous hydrogen molecule into two hydrogen atoms that diffuse into the metal, where an ideal solution of hydrogen atoms in palladium is formed:

$$C_H = K_S P_{H_2}^{0.5} \qquad (2.2)$$

Where

C_H = hydrogen atom concentration in palladium (mol/cm^3),

K_S = Sievert's constant (atm$^{0.5}$) and

P_{H_2} = hydrogen partial pressure (atm).

The flux of hydrogen (J_{H2}) through a palladium which is twice the flux of hydrogen atoms (J_H) is expressed as:

$$J_H = 2J_{H_2} = -D\frac{\Delta C_H}{\Delta z} \tag{2.3}$$

Where

D = diffusion coefficient of hydrogen atom in the membrane (cm^2) and

Δz = membrane thickness (μm).

Combining the two equations above yields;

$$J_{H_2} = -\frac{DK_s}{2}\frac{(P_{H_2,ret}^{0.5} - P_{H_2,perm}^{0.5})}{\Delta z}\ , \tag{2.4}$$

Alternatively, Equation (2.4) can be generalized as;

$$J_{H_2} = -\frac{DK_s}{2}\frac{(P_{H_2,ret}^{n} - P_{H_2,perm}^{n})}{\Delta z} \tag{2.5}$$

Collins and Way found that the value of *n* was significantly dependent on temperature and the *n* value of a palladium layer with 17 μm thickness decreased from 0.622 to 0.552 when the permeating temperatures increased from 723K to 873K (31). Hulbert and Konecny (32) showed that the bulk diffusion of hydrogen was the rate limiting step when the thickness of the palladium layer was greater than 20 μm. Uemiya et al. (33) reported that diffusion-limited permeations extended to thicknesses less than 10 μm. There has not been agreement among experimental observations for very thin Pd films due to the complexity of the overall transport mechanism and also with difficulty in quantifying factors such as poisoning and surface contamination. Ward and Dao (7) reported that

diffusion was likely to be the rate-dominating step at moderately high temperatures ($\geq$573K), even for membrane thicknesses approaching 1 μm. Ward and Dao (7) also concluded that desorption was the rate-limiting step at low temperatures and adsorption was only likely to be important at very low hydrogen partial pressure or in the presence of substantial surface contamination. The deviation from the Sievert's law has been reported in the literature and has been attributed to a variety of reasons such as:

1. Non-steady state operation (6)
2. Poisoning of the palladium surface (7, 32, and 34)
3. Grain boundaries (5)
4. Accumulation of non-diffusing gases on the upstream side of the membrane (32)
5. Different rate limiting step (6), and
6. Transport resistance of the support layer (35)

The transport resistance of the support is considered to be negligible in most permeability studies, but Huang et al (35) in their studies showed that considerable transport resistance can exist in the support layer also. Burggraaf (36) in his work reported that the mass transfer resistance associated with the Knudsen diffusion or viscous flow through the porous support could be very significant in a composite membrane.

The purpose of the present thesis is to develop a mechanistic model of hydrogen permeation in the Pd/ alumina composite membrane fabricated at UTSI. The concepts

and model description of each step involved in the hydrogen permeation are next reviewed in detail.

3. PERMEATION THEORY AND MODEL FORMULATION

A schematic of the hydrogen permeation measurement system used in prior permeation measurements at UTSI is shown in Figure 1 (9). A magnified schematic of the Pd/alumina composite membrane holder is also shown in Figure 2. In Figure 2, the reactants containing a mixture of gases were introduced in the high partial pressure side and only hydrogen permeates the membrane to the low partial pressure side of the membrane where it was carried away by the flowing nitrogen as carrier gas.

The following assumptions were taken into account to develop the mechanistic model:

1. Membrane is isothermal.
2. Flow through the membrane is laminar.
3. Steady state operation.
4. Thermodynamic equilibrium between atomic and molecular hydrogen in the dissolution transition.

The permeation of hydrogen through the Pd/ alumina composite membrane consists of the permeation through the dense palladium layer followed by the permeation through the porous alumina layer. A detailed description of the permeation process in each layer is discussed below.

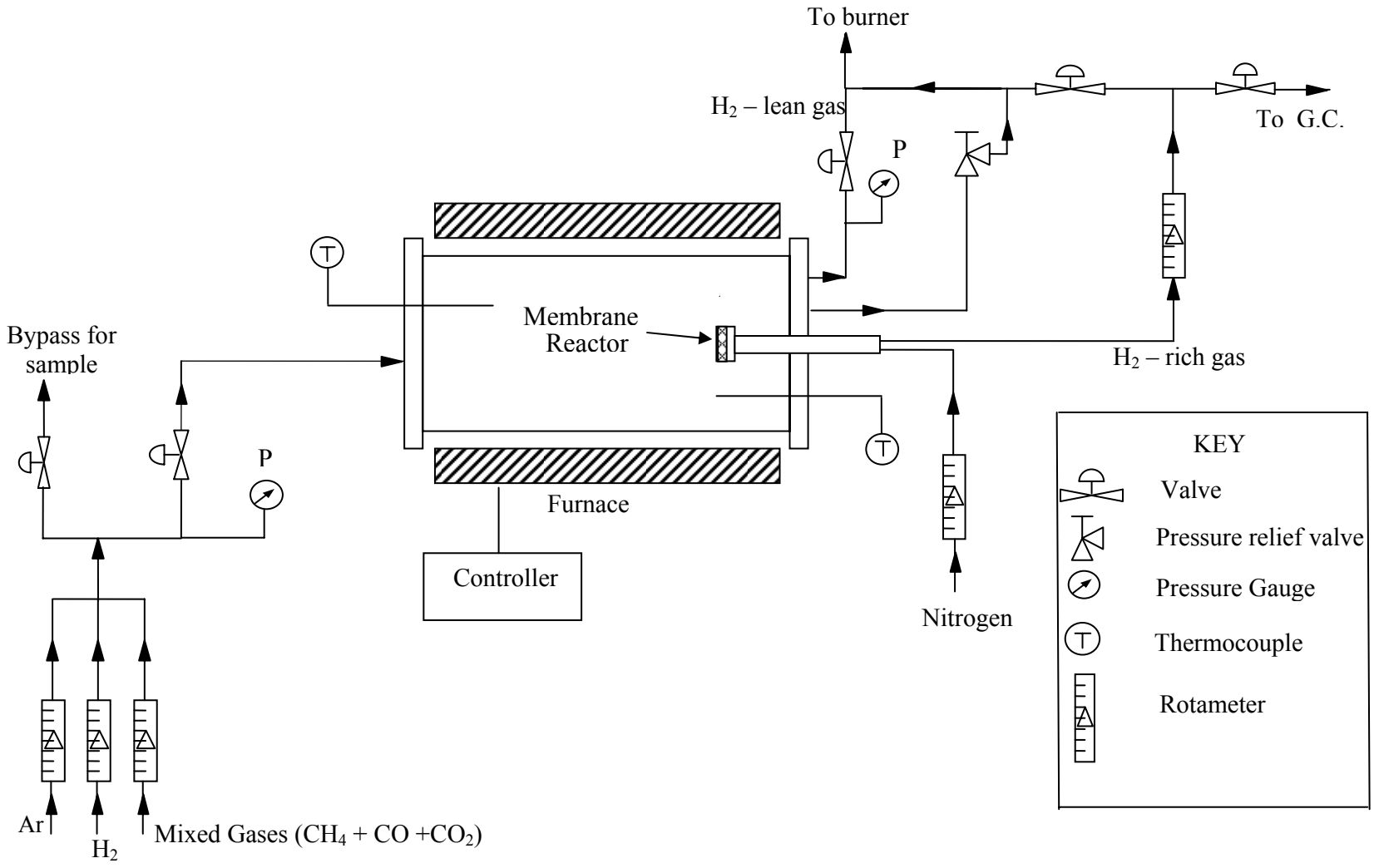

Figure 1 Schematic of experimental setup to measure permeability of H_2 (9)

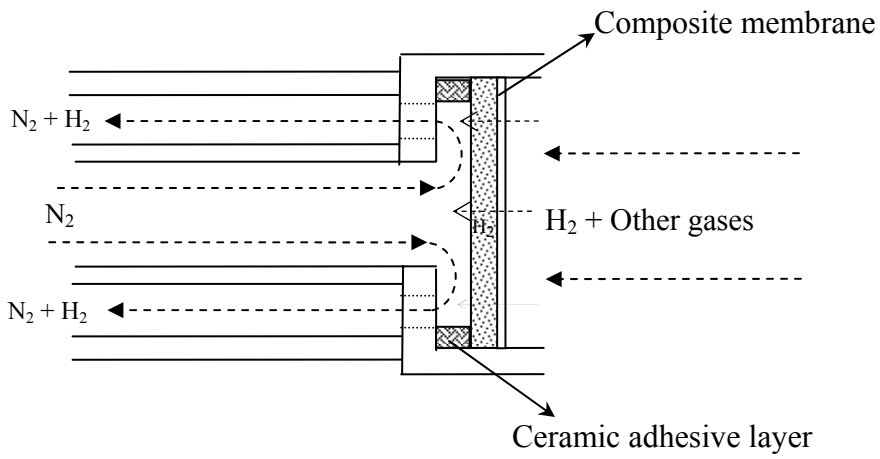

Figure 2 Schematic of gas flow for Pd/ alumina composite membrane holder (9)

3.1 Hydrogen Permeation in Palladium

The mechanisms of hydrogen permeation through a palladium membrane have been studied extensively (6, 7, 19, and 20). These are listed below in order from the high partial pressure side to the low partial pressure side (see Figure 3):

1. molecular transport from the bulk gas to the gas layer adjacent to the Pd surface,
2. dissociative adsorption onto the Pd surface,
3. transition of atomic H from the Pd surface into the bulk Pd metal,
4. atomic diffusion through the bulk Pd metal,
5. transition from the bulk Pd metal to the Pd surface on the low partial pressure side,
6. associative desorption from the low pressure side Pd surface, and
7. gas transport away from the low pressure side surface to the bulk gas.

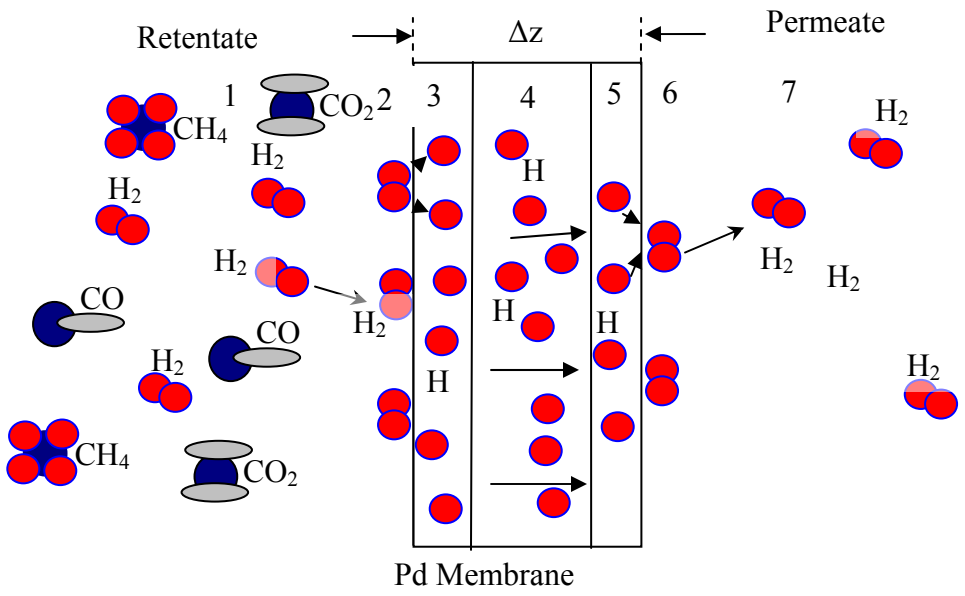

Figure 3 Mechanism of H2 transport through Pd layer

Steps 2, 3, 5 and 6 are reversible and take place on both faces of the membrane. The overall observed rate of permeation may be limited by one step if it is the slowest step or may be governed by a combination of steps. Appropriate rate expressions and parameters for each step will be examined below (7). All rate quantities are expressed in terms of atomic hydrogen flux, except where noted, and thus flux quantities have units of mol H/ (area × time). Equilibrium between molecular and atomic hydrogen is given by:

$$H_2 \rightleftarrows 2H \qquad (3.1)$$

Hence, the flux of hydrogen atom (J_H) is estimated to be twice that of hydrogen molecules.

Figure 4 shows a schematic of energy level diagram for Pd-H system, adapted from the work of Ward and Dao (7) and similar to those postulated by Picks (37).

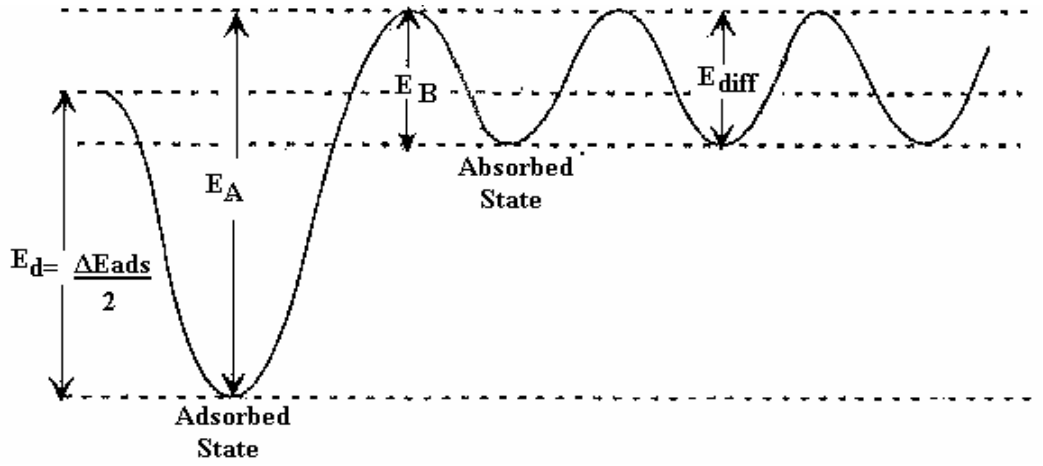

Figure 4 Energy level diagram used to model H permeation through Pd (7).

Figure 4 displays activation energies defining the surface barrier model for hydrogen adsorption/desorption in palladium metal. E_d is the activation energy for H atom desorption (kcal/mol H) and is half the value of the heat of adsorption, ΔE_{ad} (kcal/mol H_2). E_A is the activation energy for surface-to-bulk Pd metal transition (kcal/mol H). E_B is the activation energy for H atom bulk Pd metal-to-surface transition (kcal/mol H). E_{diff} is the activation energy for H atom diffusion in Pd (kcal/mol H) and is essentially the same as the bulk Pd metal-to-surface activation barrier. These activation energies will be used in our work for calculations in the different mass transfer steps.

3.1.1 Film Transfer

This is the external mass transfer resistance associated with the molecular transport from the bulk gas to the gas layer adjacent to the Pd surface. In this case the resistance to mass transfer is assumed to reside in a gas film in the fluid next to the surface. The flux from

the bulk gas phase to the surface of the Pd membrane using a mass transfer coefficient can be expressed as:

$$J_H = 2h(C - C_s) \tag{3.2}$$

and

$$h = \frac{D_{H_2}}{\delta} \tag{3.3}$$

Where

J_H = atomic hydrogen flux (mol/cm^2 s),

h = mass transfer coefficient (cm/s),

C = gas phase molecular hydrogen concentration in the bulk (mol/cm^3),

C_s = gas phase molecular hydrogen concentration adjacent to the surface (mol/cm^3),

D_{H2} = diffusion coefficient of hydrogen gas in the bulk (cm^2/s), and

δ = thickness of the film (cm).

The diffusion coefficient of hydrogen in a mixture of gases, D_{H2m}, can be gotten from the equation (38):

$$D_{H_2m} = -\frac{J_{H_2} - x_{H_2} J_{H_2} - x_{H_2} \sum_{i=2}^{n} J_i}{\sum_{i=2}^{n} \frac{x_{H_2} J_i - x_i J_{H_2}}{D_{H_2 i}}} \tag{3.4a}$$

Where

J_{H2} = molecular hydrogen flux (mol/cm^2 s),

x_{H2} = mole fraction of hydrogen in the gas mixture,

i = all other components in the gas mixture,

n = number of components in the gas mixture,

J_i = molecular flux of the other gas components (mol/cm^2 s),

x_i = mole fraction of the other gas components in the gas mixture, and

$D_{H_2 i}$ = diffusion coefficient of hydrogen in each of the other gas components present in the mixture of gases. For gasification reaction, multi-component stream consist of H_2, CH_4, CO and CO_2.

An approximation to equation (3.4a) can be obtained by assuming H_2 to be diffusing through a stagnant mixture. Expansion of Equation (3.4a) for diffusion of hydrogen through a stagnant mixture of CH_4, CO and CO_2 becomes:

$$D_{H_2} = \frac{1 - x_{H_2}}{x_{CH_4} / D_{H_2-CH_4} + x_{CO} / D_{H_2-CO} + x_{CO_2} / D_{H_2-CO_2}} \qquad (3.4b)$$

The external resistance to mass transfer has been neglected in our work because of the inability to accurately predict the gas film thickness adjacent to the surface (38) and also to allow the effects of surface versus bulk processes in Pd to be observed without the complication of external film mass transfer resistance (7). The gas phase hydrogen concentration is related to partial pressure by the ideal gas law:

$$C = \frac{P}{RT}$$

C and C_s were taken to be equal in this model as a result of neglecting the gas phase film mass transfer.

3.1.2 Dissociative Adsorption at the Surface

The reaction scheme for the hydrogen was formulated by C. Wagner about 40 years ago as follows (8):

$$H_{2,gas} + 2* \underset{k_1'}{\overset{k_1}{\rightleftharpoons}} 2H_{ad,} \tag{3.5}$$

$$H_{ad} \underset{k_2'}{\overset{k_2}{\rightleftharpoons}} H_{Me} + *. \tag{3.6}$$

H_{Me} denotes a hydrogen atom in the bulk metal, H_{ad} in the (atomic) chemisorbed site and * a free adsorption site. The atomic adsorption rate of hydrogen on the Pd surface is represented by the following expression (7):

$$\text{Adsorption rate (mol H/cm}^2\text{ s)} = 2S(\theta)\Gamma \tag{3.7}$$

Where

θ = fractional surface coverage (surface H/Pd atomic ratio),

$S(\theta)$ = coverage-dependent sticking coefficient, and

Γ = molecular bombardment rate (mol H_2 /cm^2 s) and is given by the kinetic theory of gases as:

$$\Gamma = C_s(RT/2\pi M_{H_2})^{0.5} \tag{3.8}$$

Where

M_{H2} = molecular weight of hydrogen (g/mol),

C_s = molecular hydrogen concentration (mol/cm^3),

T = temperature (K), and

R = gas constant (g.cm^2/s^2.mol.K).

The existence of structural order in the adsorbed layer is quantitatively introduced into the kinetic model through a parameter θ_{00}, which is the probability of two empty sites being next to each other (7, 40). An expression for θ_{00} based on the quasi-chemical equilibrium approximation has been given as (7, 40):

$$\theta_{00} = 1 - \theta - \frac{2\theta(1-\theta)}{[1 - 4\theta(1-\theta)(1-\exp(-\omega / kT))]^{0.5} + 1} \qquad (3.9)$$

Where

ω = pairwise interaction energy.

k = Boltzmann's constant.

The pairwise interaction energy, ω, is the energy change taking place in the process indicated schematically as

2OA→ OO + AA,

where O, A, OO, AA and OA represent unoccupied site, occupied site, adjacent unoccupied site pair, occupied pair and unoccupied/occupied pair, respectively (40). The "equilibrium constant" for the process is equal to ¼exp (-ω/kT), where the factor 4 arises from the fact that the symmetry numbers of OO and AA are 2. Hence the equilibrium distribution of adsorbate in the chemisorbed layer can be described by the equation (40):

$$N_{oo} N_{AA} / N_{OA}^2 = \frac{1}{4} \exp(-\omega / kT) \qquad (3.10)$$

Where

N_{00} = number of unoccupied pairs per unit area,

N_{AA} = number of occupied pairs per unit area, and

N_{0A} = number of unoccupied/occupied pairs per unit area.

In equation (3.9), 1-exp (-ω/kT) is defined as B, and this B possesses the limit of $0 \leq B \leq 1$, where B = 0 corresponds to -ω/T = 0 and hence complete disorder while B = 1 corresponds to $\omega/T = \infty$ and represents a perfect order (40). Since the probability of existence of two empty sites is the ratio of the coverage-dependent sticking co-efficient to the initial sticking coefficient (at zero coverage), we have

$$S(\theta)/S_0 = \theta_{00} \qquad (3.11)$$

If there is no short range order in the chemisorbed layer, B = 0, and from equations (3.9) and (3.11) we get

$$S(\theta)/S_0 = (1-\theta)^2 \qquad (3.12)$$

This is the Langmuir expression for dissociative adsorption (40). But, if there is a large repulsive interaction energy such that B = 1, then from equation (3.9) and (3.11) we get

$S(\theta)/S_0 = (1 - 2\theta)$ for $\theta \leq 0.5$, and

$S(\theta) = 0$ for $\theta \geq 0.5$, (3.13)

For our work, the Langmuir isotherm (equation 3.12) was used because hydrogen undergoes chemisorption as atomic hydrogen and gives localized mono-layers, which at equilibrium, seems to follow Langmuir's isotherm, leading to the sticking expression given by equation (3.12) (39) . The term $(1-\theta)^2$ implies that every single hydrogen molecule which impinges on the surface will dissociate and be chemisorbed provided it finds two empty sites at the surface. This form has been used in prior modeling of

hydrogen absorption and permeation in palladium (6, 34, 37, 39). The constant S_0 which is the sticking coefficient at zero coverage is generally regarded to be near unity for clean Pd surface (6, 7, 11, 37, 44), and the same was assumed in our model also.

3.1.3 Surface-to-Bulk Transition in Palladium Metal

The flux from the adsorbed surface state on the high pressure gas side into the bulk Pd metal is given by (7):

Surface-to-bulk Pd metal rate (mol H/cm^{2}s) = $N_s N_b \upsilon_d \theta \ (1 - X_{1s})$ (3.14)

Where

N_b = bulk Pd atomic concentration (mol Pd/cm^3),

X_{1s} = H/Pd atomic ratio in the bulk metal adjacent to the upstream surface, and

N_s = Pd atom surface concentration (mol Pd atoms/cm^2), which can be expressed as

$N_s = N_b^{2/3} / N_{av}^{1/3}$ (3.15)

Where N_{av} is the Avogadro's number,

υ_d is the activated rate constant for the surface-to-bulk transition, and is given by (7);

$\upsilon_d = \upsilon_0 \exp(-E_A/RT)$ (3.16)

Here, υ_0 is the pre-exponential factor for υ_d, and its impact will be discussed later.

The flux is dependent on the surface coverage and on the surface concentration of hydrogen atoms. The fact that this flux is proportional to the surface coverage, θ, indicates that the species entering the bulk Pd-metal are individual hydrogen atoms and not hydrogen molecules. E_A is the activation energy for surface-to-bulk metal transition and was estimated based on the relationship (7)

$E_A - E_B = (\Delta E_{ad} - \Delta E_{ab})/2$ (3.17)

Here E_B is the activation energy for the bulk metal-to-surface transition (kcal/mol H) and it is taken to be equal to the activation energy for diffusion (5.45 kcal/mol H, as discussed below), ΔE_{ad} and ΔE_{ab} are the heats of adsorption and absorption, respectively, in kcal/mol H_2. Values of these parameters were estimated from the literature, (11, 12, 41), and were ΔE_{ad} = 20.0 kcal/mol H_2, ΔE_{ab} = 4.0 kcal/mol H_2 and E_B = 5.45 kcal/mol H, which yielded a value of E_A = 13.45 kcal/mol H. The standard values of N_b = 0.113 mol Pd/cm^3 and $N_s = 2.8\times10^{-9}$ mol Pd/cm^2 were used for the model and were also taken from the literature values (7).

3.1.4 Solid State Atomic Hydrogen Diffusion

Within the bulk palladium metal, there is an atomic hydrogen diffusion flux per unit area through the membrane. The atomic diffusion flux through the bulk palladium was modeled using the linear one-dimensional Fickian expression (7):

Diffusion flux (mol H/cm^{2}s) = $DN_b(X_1 - X_2)/\Delta z$ (3.18)

Where

Δz = membrane thickness (cm), and

X_1 and X_2 = the bulk H/Pd atomic ratios adjacent to the upstream and downstream surfaces, respectively.

Equation (3.18) is only valid for thin membrane or where the internal diffusion coefficient is constant.

Mass transfer resistance between the surface and the bulk of palladium metal film was neglected thereby assuming that $X_1 \approx X_{1s}$ and $X_2 \approx X_{2s}$.

The hydrogen-in-palladium diffusion coefficient, D is expressed as (7):

$$D = D_0 \exp(- E_{diff} / RT) \quad (3.19)$$

Where E_{diff} = the activation energy of H atom diffusion in Pd.

There are some variations in the values for hydrogen diffusion in palladium reported by a number of researchers (3, 22 – 26). A linear regression of the different values reported in the literature was carried out using equation (3.19), and based on that, the values of D_0 = 3.3 x 10^{-3} cm^2/s and E_{diff} = 5.45 kcal/mol H were obtained and used in the model. The impact of these parameters on the predicted hydrogen transport will be discussed later. The thickness of the palladium layer in the composite Pd/Al_2O_3 membrane used for this study was taken to be equal to 77μm (9) and was incorporated in the model.

In the material science literature, it has been reported that both bulk diffusion and grain boundary diffusion takes place within a material. Grain boundary diffusion has been found to be faster than bulk diffusion in most of the materials and therefore, grain boundary diffusion is dominant/faster at the beginning of diffusion and at high temperature which saturates in very short time and then followed by the bulk diffusion. The initial grain size (grain boundary area) has a great influence on the diffusion rate. Finer size grain structure will have very rapid diffusion due to a large grain boundary area available for the purpose where as for a large grain structure; grain boundary diffusion will be insignificant (5). Grain boundary diffusion was not taken into account in this model.

3.1.5 Bulk Pd Metal-to-Surface Transition at the Low Pressure Side

The flux of hydrogen atoms from the bulk of Pd metal to the surface at the low pressure side is given by an expression similar to equation (3.14) (7):

Bulk-to-surface rate (mol H/cm^{2}s) = $N_s N_b \beta_d X_{2s} (1 - \theta)$ (3.20)

Where

X_{2s} = H/Pd atomic ratio in the bulk metal adjacent to the downstream surface,

β_d is a rate constant similar to υ_d, and it is given by

$\beta_d = \beta_0 \exp(-E_B/RT)$ (3.21)

β_0 is the pre-exponential factor similar to υ_0 and will also be discussed later.

The factor $(1 - \theta)$ implies that there must be a vacant site at the surface for the diffusing hydrogen atoms to reach the surface. The rate is also dependent on the bulk palladium metal atom concentration. In the energy level diagram shown in Figure 4, the activation energy for diffusion, E_{diff} was shown to be approximately equal to the activation energy for bulk Pd metal-to-surface transition, E_B, taken from (7). Based on this, the value of E_B = 5.45 kcal/mol H was used in the model. This assumption was supported by the fact that in the literature on desorption studies, there has been no evidence supporting kinetic limitation in the bulk-to-surface transition (7, 41).

The pre-exponential factors β_0 and υ_0 can be viewed as being related to jump attempt frequencies for the surface-bulk transitions (7). Analogy to simple solid state diffusion suggested that a reasonable value for β_0 can be estimated based on the jump frequency being related to the diffusion coefficient by (42, 43):

$$D = \alpha a^2 \Gamma_j \qquad (3.22)$$

Where

D = diffusion coefficient,

Γ_j = jump frequency,

a = lattice parameter, and

α = coefficient determined by the geometric relationship between the interstitial sites.

To estimate a reasonable value of β_0, the following was considered. Palladium has an FCC (face centered cubic) structure with a lattice parameter of 0.3890 nm (43, 44), and α value of 1/12 for the octahedral sites in the FCC lattice. The temperature dependence of Γ_j can be represented by an Arrhenius expression (7):

$$\Gamma_j = \Gamma_{j0} \exp(-E/RT) \qquad (3.23)$$

By analogy to equation (3.22), an expression relating the pre-exponential factors of D and Γ_j is then

$$\Gamma_{j0} = 12 D_0 / a^2 \qquad (3.24)$$

This gives a jump attempt frequency (Γ_{j0}) of 2.3×10^{13} s^{-1}. It is reasonable to assume that the jump attempt frequency for the bulk-to-surface transition will be approximately equal to that for diffusion in the bulk palladium because the H atom is jumping from a bulk interstitial site in both cases. One third of the interstitial jumps will be into the next (0 0 1) plane, for diffusion between (0 0 1) planes of the FCC lattice. Thus, assuming one third of the jumps from the bulk layer immediately adjacent to the surface, the diffusive jump rate is equal to $\frac{1}{3} N_s X_s \Gamma_j$, where the product $N_s X_{2s}$ is the area concentration of H

atoms in the bulk adjacent to the surface. The diffusive jump rate can be equated to equation (3.20) to give (7)

$$\tfrac{1}{3}\Gamma_{j0} = N_b\beta_0 (1-\theta) \qquad (3.25)$$

For $\theta << 1$, when surface coverage does not inhibit the bulk-to-surface transition, equation (3.25) gives $\beta_0 = 6.8 \times 10^{13}$ cm^3/mol H s. This value was used in the model.

3.1.6 Associative Desorption of Hydrogen at the Low Pressure Surface

With regard to desorption kinetics, the rate of associative desorption at the low pressure Pd surface may be expressed as (11):

$$\text{Desorption rate (mol H/cm}^2\text{ s)} = 2k_d'' N_{AA} \qquad (3.26)$$

where

k_d'' = desorption rate constant in s^{-1},

N_{AA} = concentration of nearest neighbor occupied site pairs at the surface (11). Within the quasi-chemical approximation, N_{AA} it is expressed as

$$N_{AA} = \frac{1}{2} z N_s \theta \left(1 - \frac{2-2\theta}{[1-4\theta(1-\theta)(1-\exp(-\omega/kT))]^{0.5}+1} \right) \qquad (3.27)$$

where z is the number of nearest neighbors on the surface, and it was taken to be 4.

In prior modeling (6, 34, 37, 39) associative desorption from the surface has also been described by (6, 37, 39):

$$\text{Desorption rate (mol H/cm}^2\text{ s)} = 2k_d N_s^2 \theta^2 \qquad (3.28)$$

Where k_d is the desorption rate constant in cm^2/mol-s and was given by

$$k_d = k_0 \exp(-2E_d / RT) \qquad (3.29)$$

A value for the pre-exponential factor for the second order desorption in equation (3.29) is $k_0 = 4.8 \times 10^{21}$ cm^2/mol H s, which was obtained from an estimate made by Behm et al. (11) based on thermal desorption data at low surface coverages.

In equation (3.29), E_d is the activation energy for atomic H desorption as shown in the Energy level diagram in Figure 4. It has been found to be approximately half the value of the heat of adsorption. Reported values of the heat of adsorption for hydrogen on palladium lie in the range 20 – 27 kcal/mol H_2 (11, 12, 41). A value of E_d = 10 kcal/mol ($\Delta E_{ad}/2$) has been reported by Ward and Dao (7) to give results that were more consistent with the literature permeation data, and was also used in the model for most of our calculations. The factor of 2 in the exponential accounts for the fact that two H atoms must be simultaneously desorbed to form one molecule of hydrogen, and the θ^2 factor arises because two sites must be adjacent to each other for desorption to occur. A relationship between k_d and k_d'' is obtained by requiring equation (3.26) to reduce to equation (3.28) as θ approaches zero or $\omega = 0$ (7). This gives:

$$k_d'' = k_d N_s / 2 \qquad (3.30)$$

In equation (3.27), the factor [1-exp (-ω/kT)] or B was mentioned earlier. B = 0 represented the Langmuir isotherm, and was used in our model. Equations (3.26), (3.27), (3.29) and (3.30) were used for the model.

3.1.7 Relationship between Kinetic Parameters and Thermodynamic Equilibrium

There is no well defined relationship between the bulk diffusional jump frequency and the surface-to-bulk transition frequency because the vibrational state of H atom in the surface state is presumably different from that in the bulk metal (7). However, the value of β_0 / υ_0 ratio has been estimated by Ward and Dao (7) using the comparison of the equilibrium H/Pd solubility data from literature and theoretical equilibrium relationship.

At equilibrium the rate of adsorption, equation (3.7) and the rate of desorption, equations (3.26) are equal. Similarly, the surface-to-bulk rate and the bulk-to-surface rate, equations (3.14) and (3.20), are equal. Equating and combining these expressions, and using the ideal gas law, leads to the following relationship (7):

$$\frac{1-X}{X} P_{H_2}^{0.5} = \frac{\beta_0 k_0^{0.5} N_s (2\pi M_{H_2} RT)^{0.25}}{\nu_0 S_0^{0.5}} \exp\left(\frac{E_A - E_B - E_d}{RT}\right) \tag{3.31}$$

This can be then compared with the thermodynamic relationships derived for equilibrium in the dissolution transition. The following elementary steps are assumed to occur for absorption of hydrogen from the gas phase:

$$\tfrac{1}{2} H_{2,gas} \underset{k_{-1}}{\overset{k_1}{\rightleftharpoons}} H^* \tag{3.32}$$

$$H^* \underset{k_{-2}}{\overset{k_2}{\rightleftharpoons}} [H] \tag{3.33}$$

H* and [H] refer to adsorbed states and absorbed states of hydrogen, respectively (41). k_{-1} = $P_{H_2}^{0.5}$ / (H*) and k_{-2} = (H*) / [H], and therefore, $k_{-2}\,k_{-1} = K_s$ which is Sievert's constant if the atomic concentration of hydrogen in the absorbed state, [H] is expressed as X = H/Pd. Sievert's law constant for the reaction above is expressed as:

$$K_s = \frac{P_{H_2}^{0.5}}{X} \tag{3.34}$$

Here P_{H_2} is the hydrogen partial pressure (atm.). Sievert's constant is also sometimes defined as the inverse of equation (3.34), in which case $k_2 k_1 = K_s$. Next, it is necessary to express K_s s a function of temperature.

For a single phase region, the equilibrium pressure, P_{H_2} varies with temperature (6) and is given by:

$$\ln P_{H_2}^{0.5} = \frac{\Delta\overline{G}_H}{RT} \tag{3.35}$$

$\Delta\overline{G}_H$ is the relative partial molar Gibbs free energy of dissolution of atomic H:

$$\Delta\overline{G}_H = \overline{G}_H - 0.5G_{H_2}^0 = (\overline{H}_H - 0.5H_{H_2}^0) - T(\overline{S}_H - 0.5S_{H_2}^0) \tag{3.36}$$

In the low hydrogen concentration region where the Sievert's law applies, the solution is considered to be ideal, and therefore,

$$\Delta\overline{G}_H = \Delta\overline{H}_H^0 - T(\Delta\overline{S}_H^0 + \overline{S}_H^{c(ideal)}) \tag{3.37}$$

$\Delta\overline{H}_H^0$ and $\Delta\overline{S}_H^0$ are the relative partial molar enthalpy and entropy of dissolution at infinite dissolution respectively, and $\overline{S}_H^{c(ideal)}$ is the configurational entropy and given by:

$$\bar{S}_H^{c(ideal)} = -R\ln\frac{X}{1-X} \tag{3.38}$$

Substituting equation (3.38) into equation (3.37), we have

$$\Delta\bar{G}_H = \Delta\bar{H}_H^0 - T\Delta\bar{S}_H^0 + RT\ln\frac{X}{1-X} \tag{3.39}$$

Equations (3.35) and (3.39) can be equated to give

$$RT\ln\left(P_{H_2}^{0.5}\frac{1-X}{X}\right) = \Delta\bar{H}_H^0 - T\Delta\bar{S}_H^0 \tag{3.40}$$

For X<<1, which has been shown (7) to be a reasonable approximation under typical membrane permeation conditions, $1 - X \approx 1$ and the left hand side becomes $RT\ ln(P^{0.5}/X)$. Substituting equation (3.40) in equation (3.34) for X<<1, an expression for K_s may then be obtained as:

$$K_s = \exp\left(\frac{\Delta\bar{H}_H^0}{RT} - \frac{\Delta\bar{S}_H^0}{R}\right) \tag{3.41}$$

The data of Holleck (23), give ($\Delta\bar{H}_H^0$ = 2000 cal/mol and $\Delta\bar{S}_H^0$ = 11.65 cal/mol K) which were reported for α-Pd with X<<1 at moderately elevated temperatures. With these data, equation (3.41) becomes:

$$K_s = \exp\left(\frac{-2000}{RT} + \frac{11.65}{R}\right)$$

$$= 352.75\exp\left(\frac{-1007}{T}\right) \tag{3.42}$$

Here, T is temperature in Kelvin and the units of K_s are $atm^{0.5}$. With X<<1, equation (3.31) becomes;

$$K_s = \frac{P_{H_2}^{0.5}}{X} = \frac{\beta_0 k_0^{0.5} N_s (2\pi M_{H_2} RT)^{0.25}}{\nu_0 S_0^{0.5}} \exp\left(\frac{E_A - E_B - E_D}{RT}\right) \qquad (3.43)$$

Equating the right hand side of equations (3.42) and (3.43), and assuming that the exponential terms are equal based on the fact that the activation energy of equation (3.42) is equal to that in equation (3.43), we get:

$$351.6 = \frac{\beta_0 k_0^{0.5} N_s (2\pi M_{H_2} RT)^{0.25}}{\nu_0 S_0^{0.5}} \qquad (3.44)$$

Substituting parameter values that have already been defined in equation (3.44) leads to the following expression for the ratio of β_0/υ_0 (7):

$$\frac{\beta_0}{\nu_0} = \frac{10.154}{T^{0.25}} \qquad (3.45)$$

Using the previously derived value for β_0, the value of υ_0 was determined using equation (3.45) as a function of temperature.

$$\nu_0 = \frac{\beta_0 \times T^{0.25}}{10.154} \qquad (3.46)$$

3.2 Hydrogen Gas Permeation in the Porous Alumina Support

In the composite Pd/Al_2O_3 membrane, 20 mm diameter porous alumina disk of 38% porosity and with 0.5 μm average pore diameter, about 4 mm thick, were used as the porous support (9). The permeation of gases through a porous media consists of Knudsen diffusion and Poiseuille flow. The properties of gas flow in the porous media depend on the ratio of the number of molecule-to-molecule collisions to that of the molecule-to-wall

collisions. The Knudsen number, K_n, is a characteristic parameter used to determine the relative contribution of Knudsen diffusion to the Poiseuille flow on the overall transport rate. K_n is defined as the ratio of the mean free path of the gas molecules, λ, to the pore radius of the medium, r, which is (2):

$$K_n = \frac{\lambda}{r} \tag{3.46}$$

where

$$\lambda = \left(\frac{16\mu}{5\pi P_m} \right) \left(\frac{\pi RT}{2M_{H_2}} \right), \tag{3.47}$$

P_m = average pressure across the medium,

μ = gas viscosity,

T = absolute temperature,

M_{H_2} = gas molecular mass, and

R = universal gas constant.

If the Knudsen number is much larger than unity, that is $K_n >> 1$, the gas molecules collide with the pore walls much more frequently than with each other and Knudsen flow results. If the Knudsen number is much smaller than unity, that is, $K_n << 1$, then Poiseuille flow is the dominant transport mechanism. However, the transition region between Knudsen and Poiseuille transport occurs mainly in the range $0.01 < K_n < 10$ and the Knudsen number for porous alumina support has been reported to fall in the transition region. The Knudsen number for our model was about 0.39 which is within the range reported in the literature for porous alumina support.

The rate of gas permeation per unit area or gas flux, J, is expressed by Darcy's law as:

$$J = F_P(P_h - P_l) \tag{3.48}$$

This flux is the molecular hydrogen gas flux since hydrogen diffuses as molecules through the porous alumina media. F_P is the permeability and P_h and P_l are the partial pressures of H_2 gas in the high pressure and low pressure sides respectively (2). In the work of Huang et al (35), it has been reported that the permeation of gases through porous media was mainly combined Poiseuille and Knudsen flow.

3.2.1 Poiseuille Flow

When the number of intermolecular collisions is strongly dominant ($K_n << 1$), the flux can be described by a Hagen-Poiseuille type flow equation (36):

$$J_V = -\frac{r^2}{8\mu}\frac{P}{RT}\frac{dP}{dZ} \tag{3.49}$$

In real porous media, equation (3.49) must be modified to account for the porosity, ε, and the complexities of the pore structure (tortuosity, τ). This gives:

$$J_V = -\frac{\varepsilon}{\tau}\frac{r^2}{8\mu}\frac{P}{RT}\frac{dP}{dZ} \tag{3.50}$$

At steady state, the fluxes into and out of any cross section of a pore are equal. Therefore (dP/dZ) is constant and the integration of equation (3.50) over the thickness L, of the porous medium gives the Poiseuille flow equation for permeability:

$$F_{PV} = -\frac{J_V}{\Delta P} = \frac{\varepsilon}{8\mu\tau}\frac{r^2}{RTL}P_m \tag{3.51}$$

Where the average pressure, $P_m = 0.5(P_l + P_h)$.

Equation (3.51) gives the permeation as proportional to the square of the pore radius and the mean pressure.

3.2.2 Knudsen Diffusion

When the number of molecule to wall collisions is strongly dominant ($K_n >> 1$), the flux can be defined by the Knudsen equation as:

$$J_K = -D_K \frac{1}{RT}\frac{dP}{dZ} \tag{3.52}$$

D_K is the Knudsen diffusion coefficient and it has been derived using the long capillary tube flow model to give (47):

$$D_K = \frac{2\bar{u}r}{3} \tag{3.53}$$

Where $\bar{u}$ is the mean molecular velocity, given by:

$$\bar{u} = \left(\frac{8RT}{\pi M}\right)^{0.5} \tag{3.54}$$

Consequently,

$$D_K = \frac{4r}{3}\left(\frac{2RT}{\pi M}\right)^{0.5} \tag{3.55}$$

In real porous media geometrical effects of pores play an important role, as discussed earlier in the viscous flow, and therefore, the Knudsen diffusion coefficient has been modified to give the effective Knudsen diffusion coefficient $D_{e,}$ as follows (47);

$$D_e = \frac{\varepsilon}{\tau} D_K \tag{3.56}$$

Substituting equation (3.56) into equation (3.52) and integrating equation (3.52) over the membrane thickness, *L*, at steady state, the Knudsen flow permeability can be expressed as:

$$F_{PK} = -\frac{J_K}{\Delta P} = \frac{D_e}{LRT} \tag{3.57}$$

Inspection of equation (3.55) shows that the Knudsen flow is dependent on the pore diameter and inversely dependent on the molecular weight of the gas.

The total permeability in the porous media can be expressed as a sum of Poiseuille flow, F_{PV} and Knudsen flow, F_{PK}:

$$F_P = F_{PV} + F_{PK} \tag{3.58}$$

Equations (3.48 – 3.58) were used in the model. Experimental tortuosity, τ, values generally fall in the region $2 < \tau < 5$ (36)), and a tortuosity value of 2.5 was used for the model calculations. This was chosen based on the fact that it gave the best results needed to simulate the experimental data from our preliminary experiments.

4. MODEL DEVELOPMENT

4.1 Model Description

The system of equations developed in chapter 3 form a model for the permeation of hydrogen gas through composite palladium/Al_2O_3 membranes. The model accounts for forward and reverse rate equations for the complete series of steps required for the transport of hydrogen from the high partial pressure side to the low partial pressure side of a composite palladium/Al_2O_3 membrane. In each step of the permeation transport process in the composite palladium membrane, the equations were set up such that the difference between the forward and reverse rate equaled the net steady state H flux. The subscript 1 and 2 signifies the high pressure side and low pressure sides respectively.

The equations used for the model are shown below in terms of atomic hydrogen flux;

1. Net adsorption rate

The net adsorption rate at the high pressure side of the membrane equaled the difference between the rate of adsorption and rate of desorption and can be written as:

$$J_H = (2S(\theta_1)C_1(RT/2\pi M_{H_2})^{0.5}) - (\frac{1}{2}k_d N_s^2 z\theta_1^2) \qquad (4.1)$$

C_1 is calculated from P_1 (hydrogen partial pressure in the feed side) using the ideal gas law and R is the ideal gas constant. M_{H_2} is the molecular weight of hydrogen with a value of 2.016.

$$S(\theta_1) = S_0(1-\theta_1)^2 \qquad (4.1a)$$

S_0 is the sticking coefficient at zero coverage and the value of 0.95 was used for our calculations based on the fact that the constant, S_0 is generally regarded to be near unity for clean Pd (6, 7, 11, 37, 44). The value of k_d was obtained from the relation;

$$k_d = k_0 \exp(-2E_d / RT) \qquad (4.1b)$$

$k_0 = 4.8 \times 10^{21}$ cm^2/mol H s, was obtained from the estimate of Behm et al. based on thermal desorption data at low surface coverages (11). A value of $E_d = 10$ kcal/mol gave results that were consistent with most literature permeation data (7), and was used for our model calculations.

2. Net surface-to-bulk Pd metal transportation rate

The flux in this step equaled the difference between the rate of surface-to-bulk Pd metal transport and the rate of bulk Pd metal-to-surface transport on the high partial pressure side of the membrane. Therefore the atomic hydrogen flux is expressed as:

$$J_H = (N_s N_b \nu_d \theta_1 (1 - X_1)) - (N_s N_b \beta_d X_1 (1 - \theta_1)) \qquad (4.2)$$

$$\beta_d = \beta_0 \, exp\,(-E_B/RT) \qquad (4.2a)$$

$$\upsilon_d = \upsilon_0 \, exp(-E_A/RT) \qquad (4.2b)$$

$$\nu_0 = \frac{\beta_0 \times T^{0.25}}{10.154} \qquad (4.2c)$$

The values of N_b =0.113 mol Pd/cm^3, $N_s = 2.8 \times 10^{-9}$ mol Pd/cm^2, β_0 =2.8 $\times$ 10^{-9} cm^3/mol H s, E_A = 15.45 kcal/mol and E_B = 5.45 kcal/mol were used for our calculations and were consistent with the literature permeation data.

3. Solid-state atomic hydrogen diffusion rate

$$J_H = DN_b(X_1 - X_2)/\Delta z \qquad (4.3)$$

$$D = D_0 \exp(-E_{diff}/RT) \qquad (4.3a)$$

Δz is the membrane thickness with a value equal to 77 μm. The values of E_{diff} = 5.45 kcal/mol and D_0 =3.3 × 10^{-3} cm^2/s were used for our calculations.

4. Net bulk Pd metal-to-surface transportation rate

The flux in this step equaled the difference between the rate of bulk Pd metal-to-surface transport and the rate of surface-to-bulk Pd metal transport on the low partial pressure side of the membrane. Therefore the atomic hydrogen flux is expressed as:

$$J_H = (N_s N_b \beta_d X_2(1-\theta_2)) - (N_s N_b \nu_d \theta_2(1-X_2)) \qquad (4.4)$$

5. Net associative desorption rate

The net desorption rate at the low pressure side of the membrane equaled the difference between rate of desorption and the rate of adsorption and can be written as:

$$J_H = (\frac{1}{2} k_d N_s^2 z \theta_2^2) - (2S(\theta_2) C_{2i} (RT/2\pi M_{H_2})^{0.5}) \qquad (4.5)$$

C_{2i} is the molecular hydrogen concentration at the Pd layer and porous alumina support interface.

6. Atomic hydrogen permeation rate in the porous alumina support

The flux in the porous alumina support was multiplied by 2 to reflect atomic hydrogen flux as molecular hydrogen diffusion at equilibrium takes place in this layer.

$$J_H = 2F_P(P_{2i} - P_2) \tag{4.6}$$

$$P_{2i} = C_{2i}RT \tag{4.6a}$$

P_2 is the molecular hydrogen partial pressure on the permeate side.

$$F_P = F_{PV} + F_{PK} \tag{4.6b}$$

$$F_{PV} = \frac{\varepsilon}{8\mu\tau}\frac{r^2}{RTL}0.5(P_{2i} + P_2) \tag{4.6c}$$

$$F_{PK} = \frac{D_e}{LRT} \tag{4.6d}$$

$$D_e = \frac{4r\varepsilon}{3\tau}\left(\frac{2RT}{\pi M_{H_2}}\right)^{0.5} \tag{4.6e}$$

The model calculations were done by numerically solving the six set of non-linear implicit equations (Equations 4.1 – 4.6) for six unknowns, θ_1, X_1, X_2, θ_2, C_{2i}, and J_H, simultaneously, using Mathematica. The "FindRoot" function, which is a built-in function used for numerical computation in Mathematica was used to search for numerical solutions to the set of non-linear simultaneous equations.

4.2 Logic Diagram/Information Flow

Figure 5 is a logic diagram/information flow chart explaining the sequential steps used in the modeling solution scheme. The input parameters are, $P_1, P_2, k_0, E_d, E_B, E_A,, R, T, L, \beta_0, N_s, M_{H2}, z, D_0, E_{diff}, \Delta z, r, \varepsilon,$ and μ. In the first step (Dissociative adsorption equation), an initial guess of H flux, J_{H0}, is put into the equation to determine the value of θ_1. θ_1 becomes an input in the second step (surface-to-bulk Pd metal rate equation) to determine the value of X_1. X_1 goes into the third step (Atomic diffusion rate equation) to determine the value of X_2. X_2 goes into the fourth step (Bulk Pd metal-to-surface rate equation) to determine the value of θ_2. θ_2 goes into the fifth step (Associative desorption rate equation) to determine the value of C_{2i}. P_{2i} is calculated from C_{2i} and then goes into the sixth step (Rate of diffusion in porous alumina support) to determine the flux, J_{Hcal}. If the value of the calculated flux, J_{Hcal} is not equal to the value of the initial guess for the flux, J_{H0}, the iteration process continues until it converges within an acceptable tolerance.

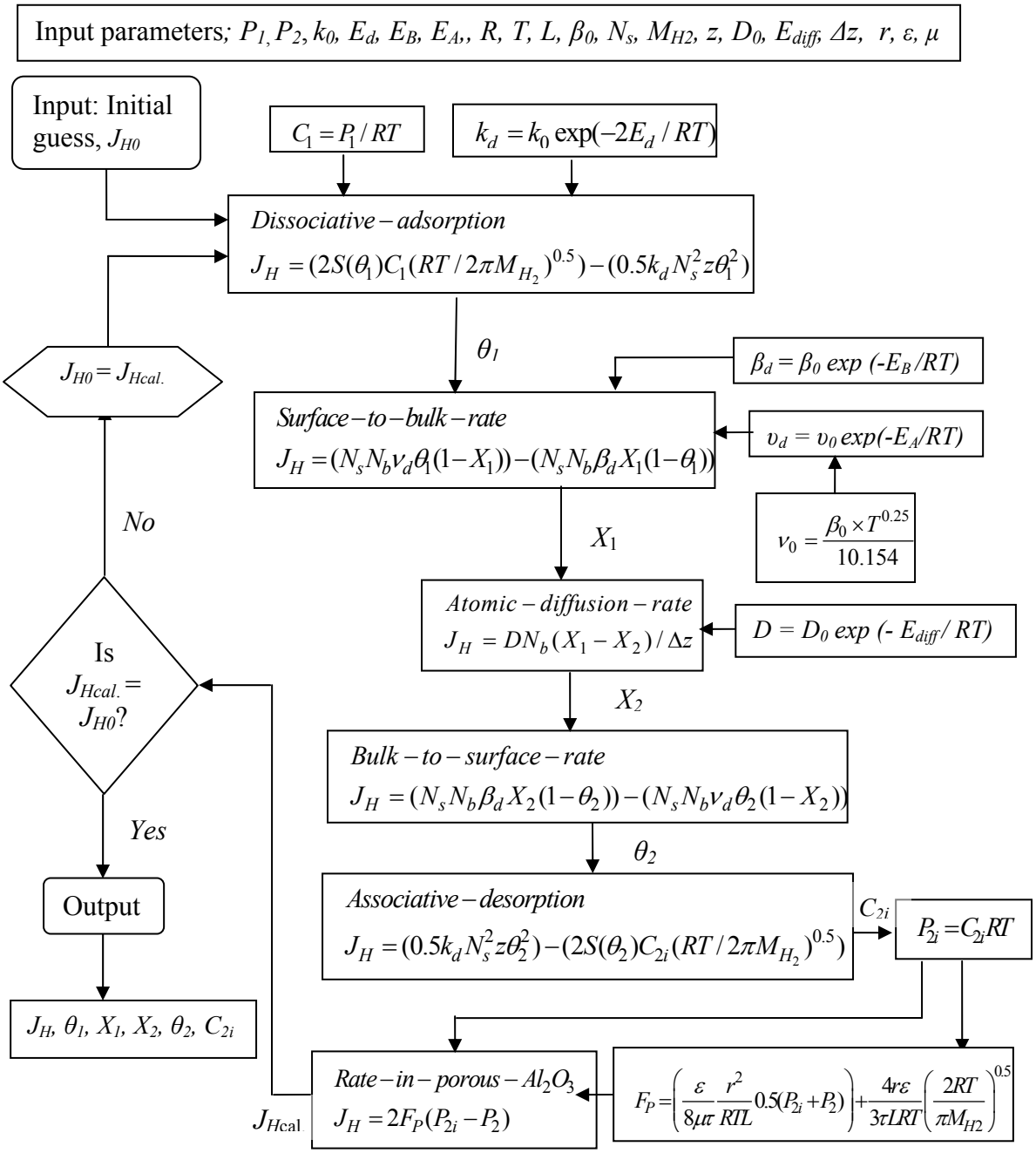

Figure 5 Information flow/ logic diagram

5. RESULTS AND DISCUSSION

5.1 Model Validation

There are four basic steps in developing a credible math model (50):

1. Develop the equations that represent the actual system.
2. Program these equations on a computer to produce a successful simulation.
3. Make sure that the computer program represents the correct simulation of the equations.
4. Compare the results of the simulation runs to the experimental data from literature and/or to ones own experimental data to validate it.

Steps 3 and 4 are commonly termed verification and validation (V & V), respectively (51, 52). Verification is the process of determining that a computer program causes the computer to operate as intended by the programmer, while validation is the process of determining that the computer simulation behaves like the actual system under study in all pertinent respects. Figure 6 below shows the relationships between the actual system, model, the computer simulation and the V & V activity.

Sargent (52) described various validation techniques to be used for model verification and validation. Two of such techniques were used in this study, they are:

1. Comparison to other models, and
2. Sensitivity analysis.

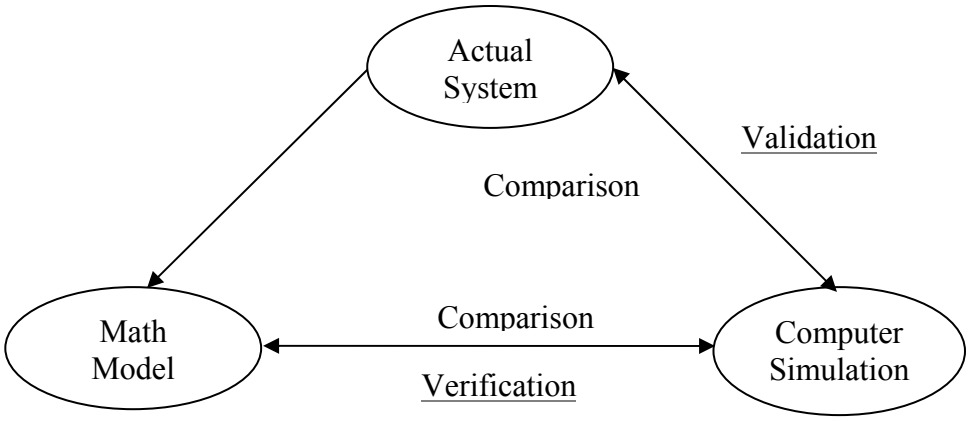

Figure 6 Relationships between system, model, simulation and verification and validation.

5.1.1 Comparison to Other Models

Various results of the simulation model being validated were compared to the results of the permeation models reported by Ward and Dao (7). Figure 7 from Ward and Dao's work was compared to Figure 8 from our model calculation and Figure 9 from Ward and Dao's work was also compared to Figure 10 from our model calculation.

In Figure 7, the solid curves are Ward and Dao's model calculations for P_1 = 1 atm, P_2 = 0, E_d = 12 kcal/mol and the thickness of palladium layer is indicated in the legend. The straight dashed lines indicate the diffusion limited flux predicted under conditions of interfacial equilibrium (Equations (3.18), (3.34) and (3.42)). A line representing the desorption-limited flux (Equation (3.28) with θ=1) is also shown.

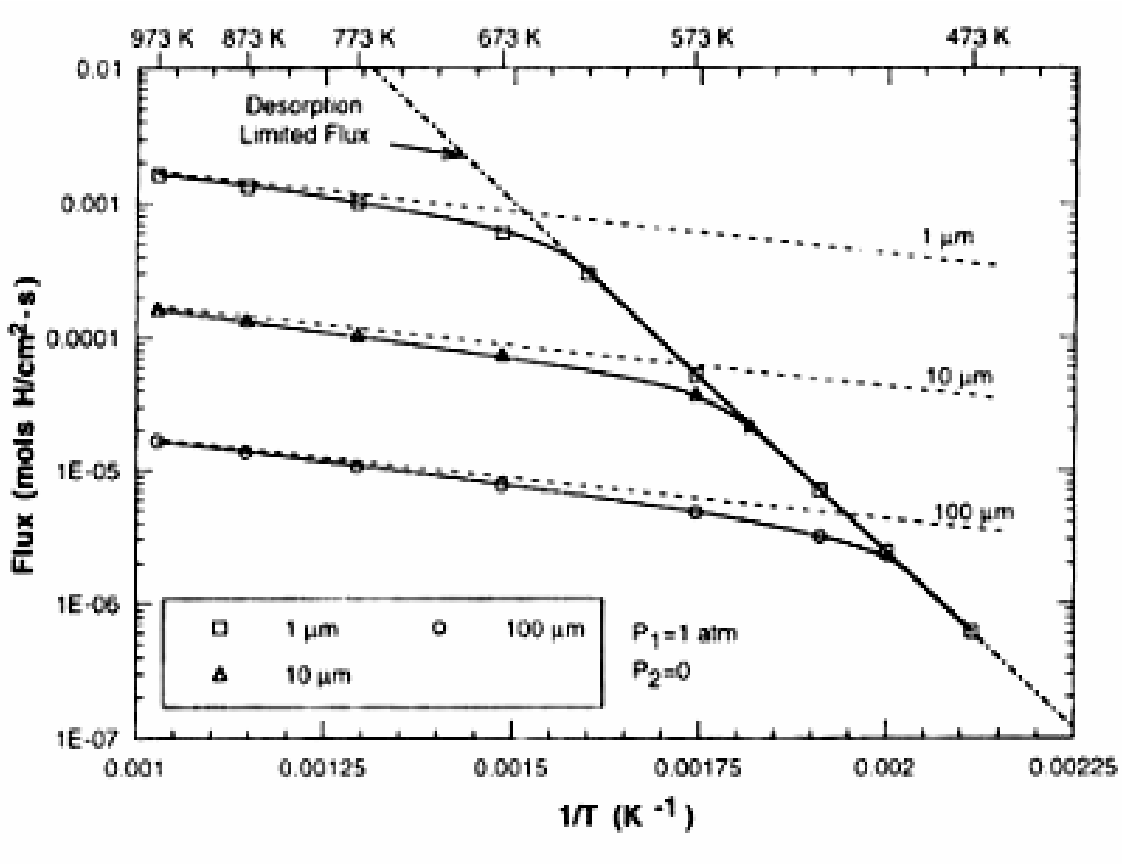

Figure 7 Plots of H atom flux versus inverse temperature for Pd membranes with external mass transfer neglected using E_d = 12 kcal/mol (7).

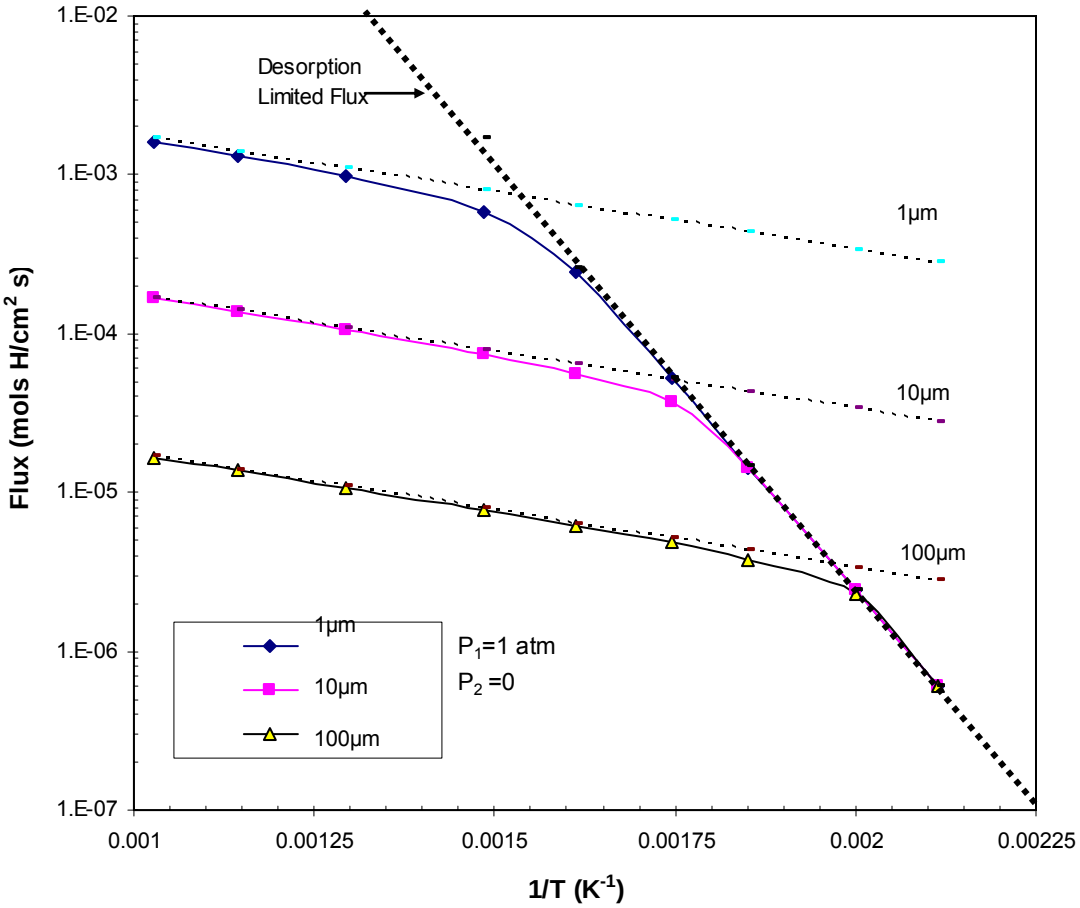

Figure 8 Our model calculations for P_1 = 1 atm, P_2 = 0, E_d = 12 kcal/mol for various Pd thickness.

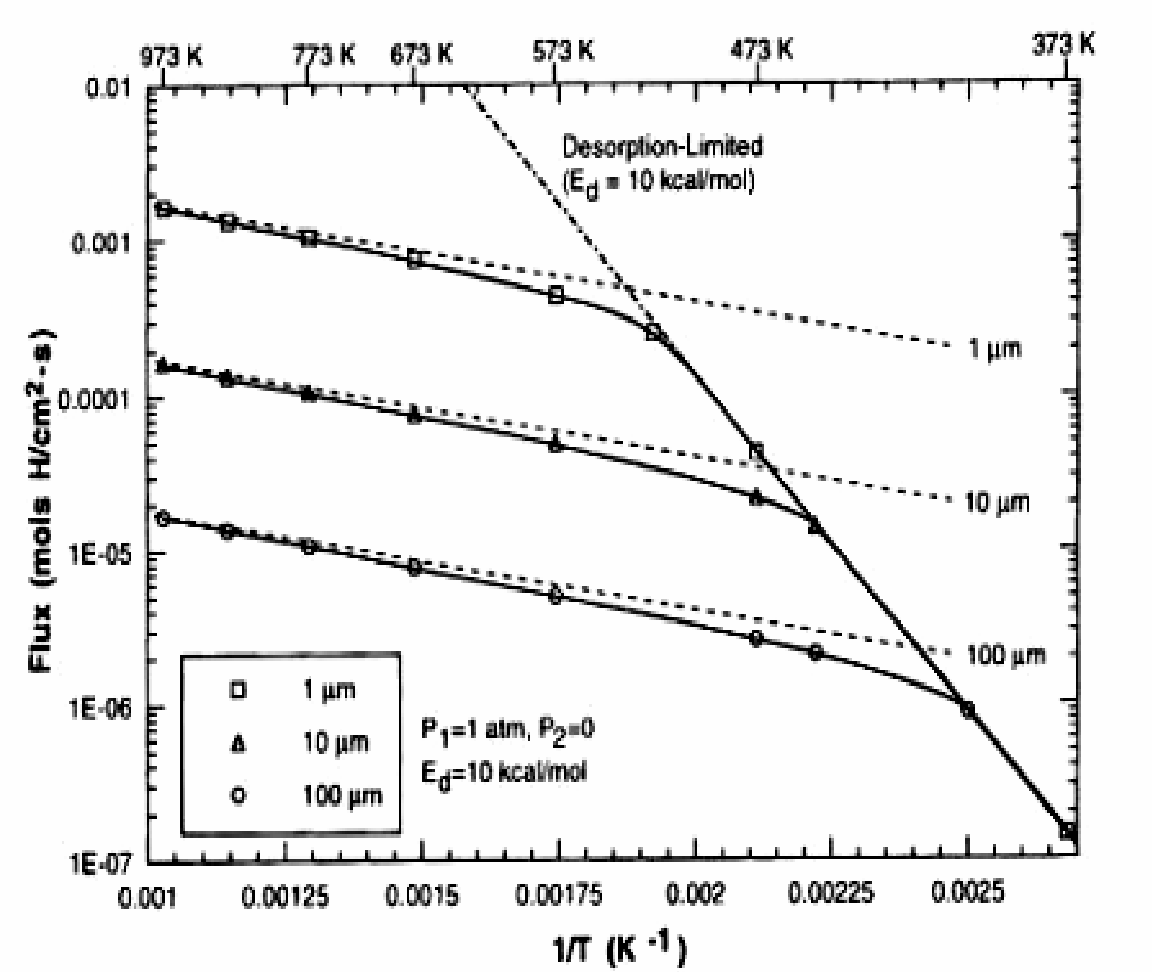

Figure 9 Plots of H atom flux versus inverse temperature for Pd membranes of different thickness using E_d = 10 kcal/mol (7).

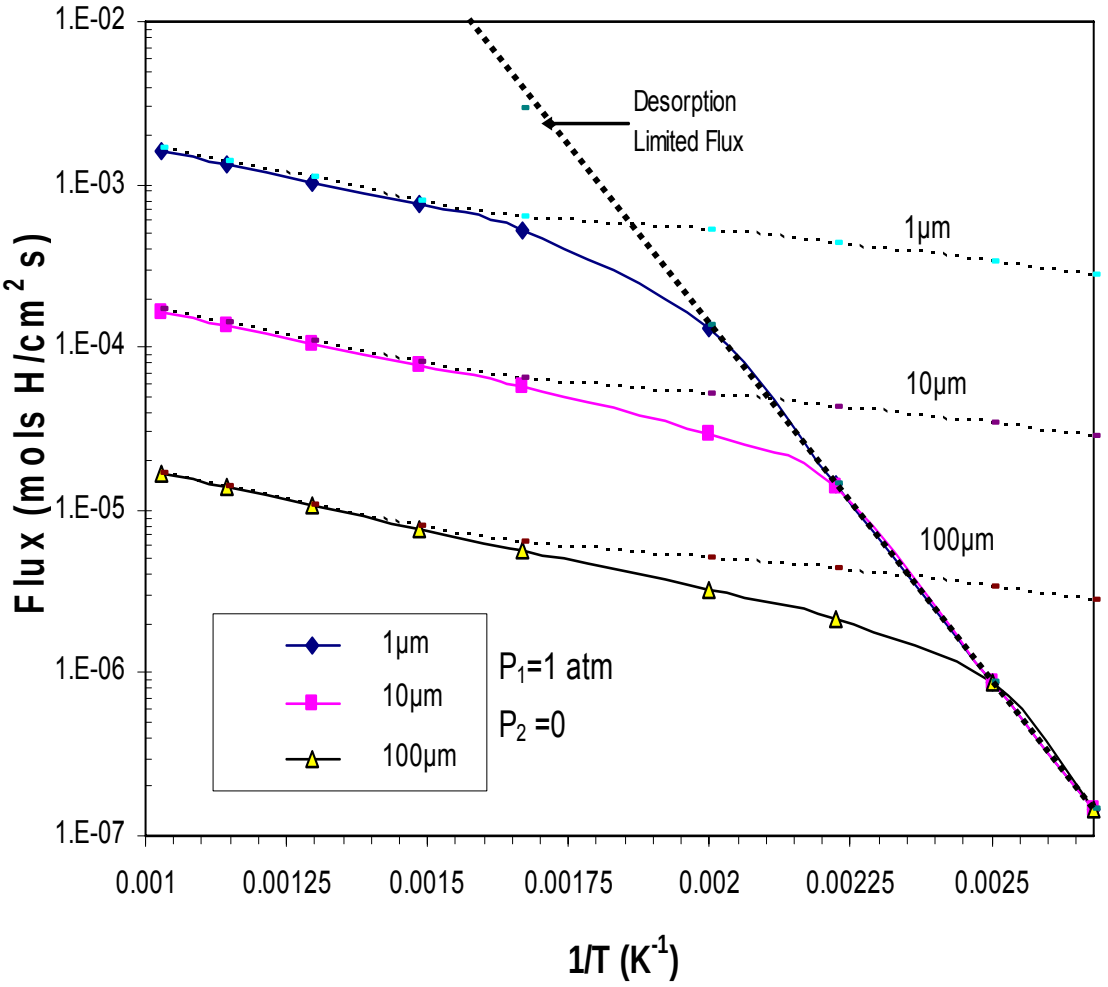

Figure 10 Our model calculations for P_1 = 1 atm, P_2 = 0, E_d = 10 kcal/mol for various Pd thickness.

In Figure 8, the solid curves are our model calculations for P_1 = 1 atm, P_2 = 0, E_d = 12 kcal/mol and the thickness indicated in the legend. The straight dashed lines indicate the diffusion limited flux predicted under conditions of interfacial equilibrium (Equations (3.18), (3.34) and (3.42)). A line representing the desorption-limited flux (Equation (3.28) with θ=1) is also shown.

Comparing Figure 7 from the Ward and Dao's work and Figure 8 from our model calculation, it is clear that the solid curves from our model calculation and diffusion-limited permeation behavior agree well with the data of Ward and Dao (7) at the different membrane thicknesses. The result of the desorption-limited flux behavior from our model calculation also shows a good match when compared with desorption limited flux data reported by Ward and Dao.

In Figure 9, the solid curves are Ward and Dao's model calculations for P_1 = 1 atm, P_2 = 0, E_d = 10 kcal/mol for the membrane thicknesses indicated in the legend. The straight dashed lines indicate the diffusion limited flux predicted under conditions of interfacial equilibrium (Equations (3.18), (3.34) and (3.42)). A line representing the desorption-limited flux (Equation (3.28) with θ=1) is also shown.

In Figure 10, the solid curves are our model calculations for P_1 = 1 atm, P_2 = 0, E_d = 10 kcal/mol for the membrane thicknesses indicated in the legend. The straight dashed lines indicate the diffusion limited flux predicted under conditions of interfacial equilibrium

(Equations (3.18), (3.34) and (3.42)). A line representing the desorption-limited flux (Equation (3.28) with θ=1) is also shown.

Again, comparing Figure 9 from the Ward and Dao's work and Figure 10 from our model calculation, it is clear that the solid curves from our model calculation and diffusion-limited permeation behavior agree well with the data of Ward and Dao (7) at different membrane thicknesses. The result of the desorption-limited flux behavior from our model calculation also shows a good match when compared with desorption limited flux data reported by Ward and Dao (7).

5.1.2 Sensitivity Analysis

This technique consists of changing the values of the input and internal parameters of a model one at a time to determine their effects on the model's behavior and its output. The same relationships should occur in the model as in a real system. For this study, sensitivity analysis was performed for the following parameters; pre-exponential factor for hydrogen diffusion coefficient in palladium, D_0; sticking coefficient at zero coverage, S_0; tortuosity, τ and the activation energy for atomic H desorption, E_d. These parameters were determined to be the important variables because they seemed to have significant influence on the calculated permeation fluxes that resulted in the preliminary calculations.

The base case parameters that were used for the sensitivity analysis are shown in Table 1. The values chosen were consistent with the literature permeation data (7). The range of the diffusion coefficient constant, $D_{0,}$ was varied from 2.3 – 4.5 cm^2/s based on the values reported in the selected literature permeation data. Table 2 presents the selected literature values for the pre-exponential factor and corresponding activation energy for the diffusion coefficient. Figure 11 shows a plot of our model calculation of atomic hydrogen flux versus pre-exponential factor for hydrogen diffusion coefficient in palladium, D_0. Figure 12 shows a plot of our model calculation of atomic hydrogen flux versus sticking coefficient at zero coverage, S_0. The range of the sticking coefficient at zero coverage, $S_{0,}$ was varied from 0.9 – 1 based on the fact that the constant, S_0 is generally regarded to be near unity for clean Pd (6, 7, 11, 37, 44). Figure 13, shows a plot of our model calculation of atomic hydrogen flux versus the tortuosity factor, τ. Tortuosity, τ, values generally fall in the region $2 < \tau < 5$ (36)) and the range for our analysis was chosen based on this. Figure 14, shows a plot of our model calculation of atomic hydrogen flux versus the activation energy for atomic H desorption, E_d. The range of E_d values, from 8 – 12.5 kcal/mol H, was used based on values reported in the literature (7, 11, 12, 41, 53). The hydrogen flux increases as D_0 increases as shown in Figures 11, which is what happens in a real system where D_0 is directly proportional to the flux. Also the H flux decreases with increased tortuosity factor as would be expected, and that trend can be seen in Figure 13.

Table 1 Summary of base case parameter values used for the sensitivity analysis

Parameter	Value
E_d	12 kcal/mol H
E_A	15.3 kcal/mol H
E_B	5.3 kcal/mol H
E_{diff}	5.3 kcal/mol H
K_0	4.8×10^{21} cm^2/mol H s
B_0	6.8×10^{13} cm^3/mol H s
D_0	2.9×10^{-3}cm^2/s
N_b	0.113 mol Pd/cm^3
N_s	2.8×10^{-9} mol Pd/cm^2
S_0	1
Y_0	Equation (3.45)
τ	2
P	2.82 atm
T	1100^{0}F

Table 2 Values of constants in the expression of the diffusion coefficient of hydrogen in palladium from the literature

Hydride phase	D_0 x 10^3 cm^2/s	E_{diff} kcal/mol	Temperature ^{0}C	References
α	2.9	5.26	260 to 640	22
α	4.5	5.76	250 to 1000	23
α	2.3	5.19	140 to 310	24
α	2.83 ± 0.05	5.4 ± 0.1	60 to 140	25
α	2.9	5.3	-40 to 600	26

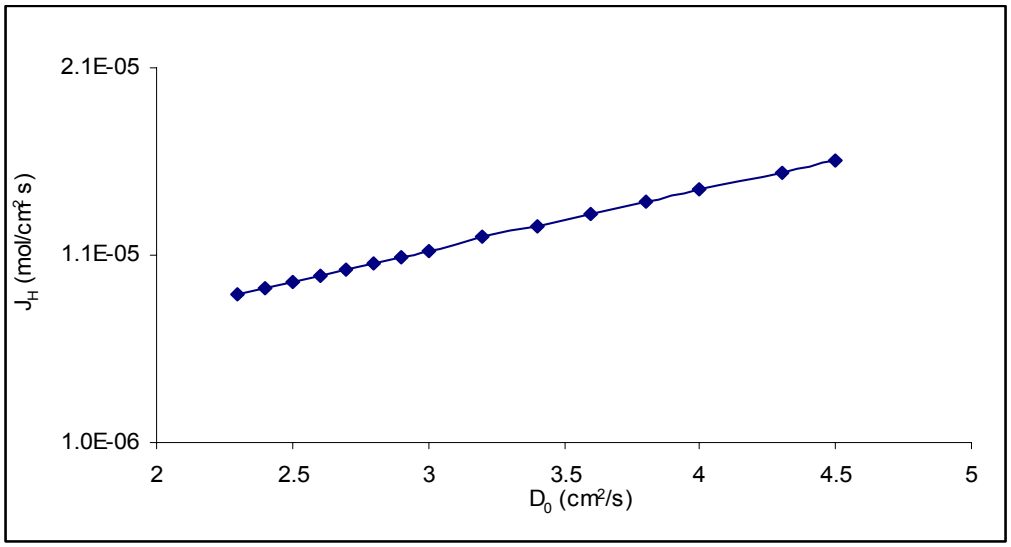

Figure 11 Model calculation of atomic hydrogen flux, J_H versus pre-exponential factor for diffusion coefficient, D_0.

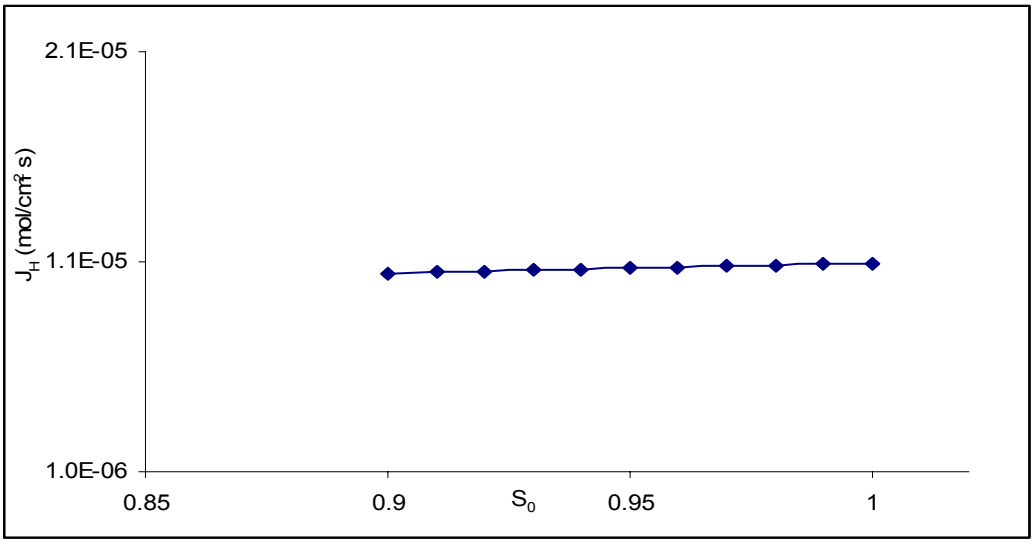

Figure 12 Model calculation of atomic hydrogen flux versus sticking coefficient at zero surface coverage, S_0.

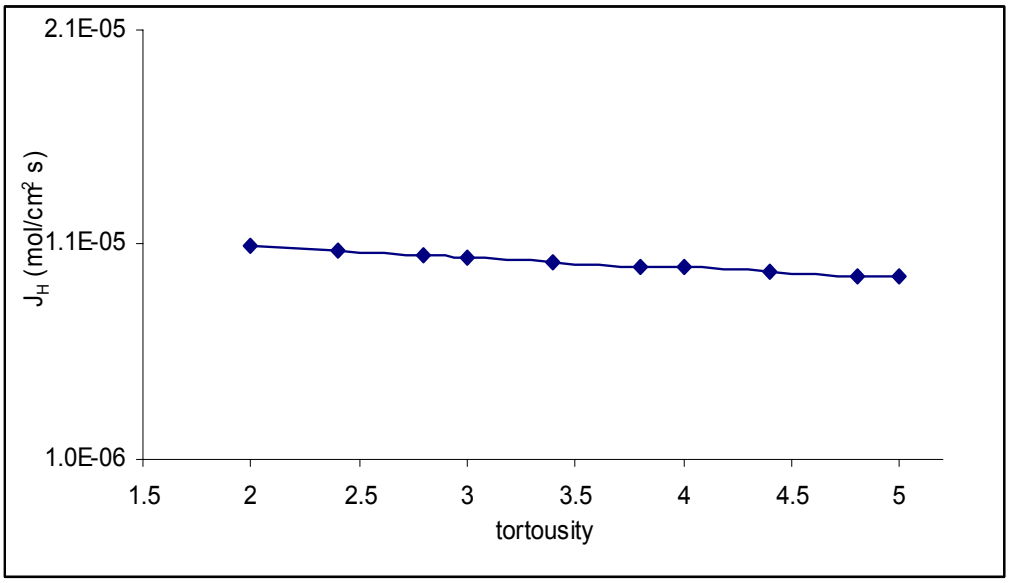

Figure 13 Model calculation of atomic hydrogen flux, J_H versus tortuosity.

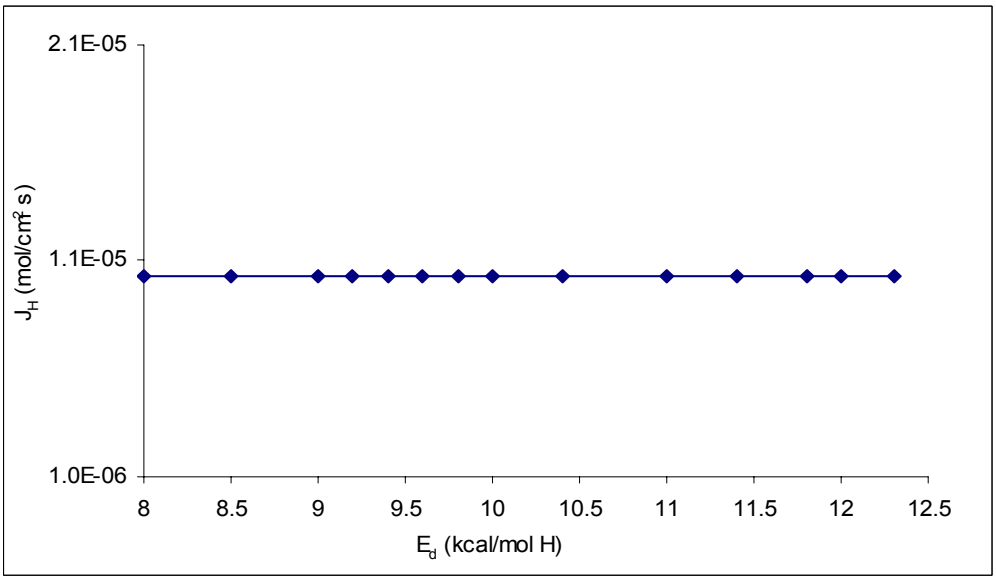

Figure 14 Model calculation of atomic hydrogen flux, J_H versus the activation energy for atomic H desorption, E_d.

From the sensitivity analyses results, the values of S_0 =0.95 was used for the model calculation based on the fact that it gave the best fit to the experimental data at 1100^0F. It also gave a maximum error band of about ± 3% in the value of J_H, based on the range of S_0 values. Similarly, tortuosity factor, τ = 2.5 was used for the model calculation based on the fact that it gave the best fit used to simulate experimental data at 1100^0F. It gave a maximum error band of about ± 10% in the value of J_H, within the range. From the sensitivity analysis, change in E_d values in the range considered did not have a significant effect on the flux value and as a result E_d = 10 kcal/mol H was used for our calculations, which is consistent with the literature permeation data. These values gave the best results needed to simulate the experimental results carried out at UTSI and gave an error band of ± 30%. This will be discussed later. Also from the sensitivity analysis, it was observed that a change in the value for the pre-exponential factor for hydrogen diffusion coefficient in palladium, D_0, had a significant effect on the H flux value. The value for the pre-exponential factor for hydrogen diffusion coefficient in palladium, D_0, was chosen based on a least square regression of D_0 values taken from the data in selected literature, given in Table 2. The data in Table 2 was expressed as equation (2.1) above:

$D = D_0 \exp(-E_{diff} / RT)$

Where

D_0 = Pre-exponential factor for the diffusion coefficient, D (cm^2/s),

E_{diff} = activation energy for H atom diffusion (kcal/mol H),

T = temperature (K), and

R = gas constant (1.987×10^3 kcal/mole K).

Taking the logarithm of the equation above gives;

$$\ln D = \ln D_0 - \frac{E_{diff}}{RT}$$

A straight line fit to the data in Table 2 was developed by plotting ln D verses 1/T as shown in Figure 15.

$\frac{E_{diff}}{R}$ = 2735.6 (slope) and $\ln D_0$ = -5.7292 (intercept), giving E_{diff} = 5.45 kcal/mol and D_0= 3.3×10^{-4} cm^2/s. As a result, the error band of ± 30% in the value of J_H was estimated (see Figure 11). These values of τ, S_0, D_0, and E_d were used for our calculation, giving an overall error band of ± 30% in the value of J_H.

Table 3 gives a summary of the final parameter values used in our model calculations. These values are not unique values because the fitting of the values to simulate experimental data was done manually.

5.2 Experimental Flux versus Model Calculated Flux

The predicted results for permeation of hydrogen in palladium composite membrane obtained with the present model were compared to experimental data (9) on permeation fluxes. One set of experimental data (at 1100°F) was used to determine the best values of the remaining but necessary parameters not selected from the sensitivity analyses. The experimental data at 1100°F was fitted by the least square analysis to minimize the square of errors.

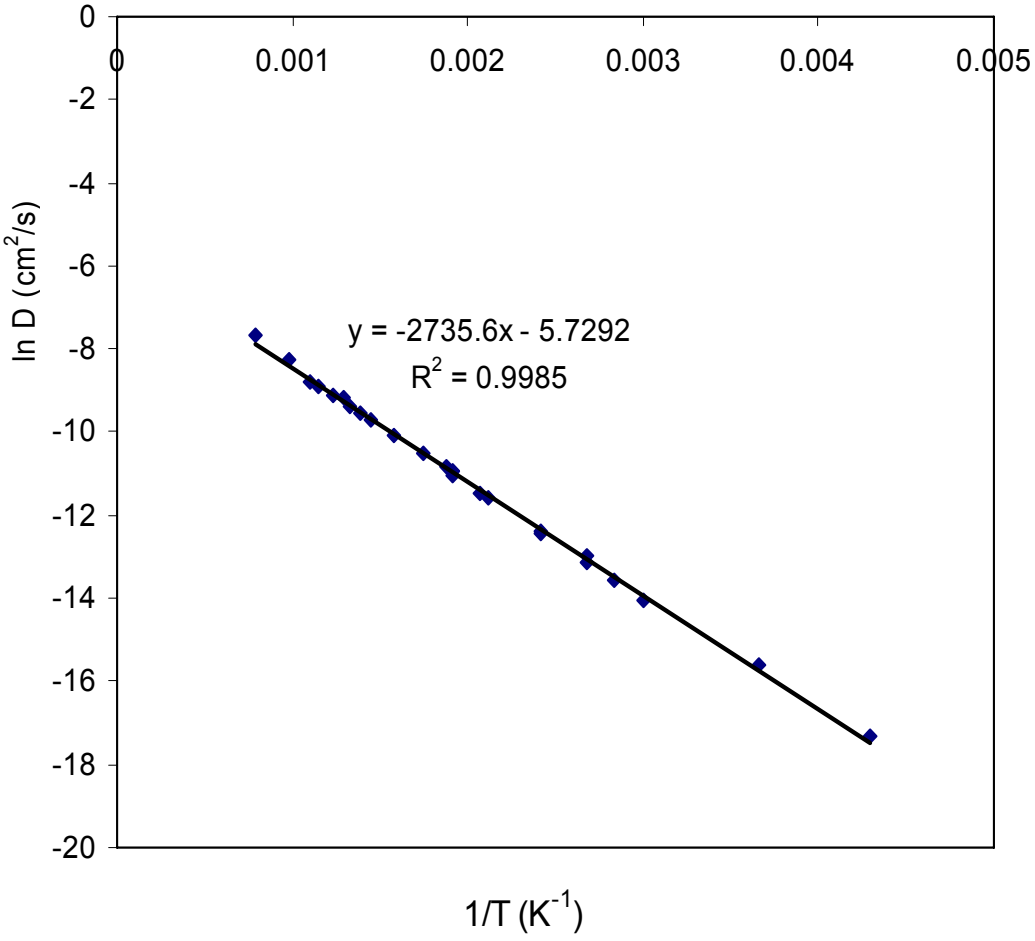

Figure 15 Plot of ln D versus inverse of temperature, (1/T).

Table 3 Summary of final parameter values used in the present model

Parameter	Value
E_d	10 kcal/mol H
E_A	13.45 kcal/mol H
E_B	5.45 kcal/mol H
E_{diff}	5.45 kcal/mol H
k_0	4.8×10^{21} cm^2/mol H s
β_0	6.8×10^{13} cm^3/mol H s
D_0	3.3×10^{-3}cm^2/s
N_b	0.113 mol Pd/cm^3
N_s	2.8×10^{-9} mol Pd/cm^2
S_0	0.95
v_0	Equation (3.43)
τ	2.5

This error was calculated using the equation:

$$\phi = \sum_{i=1}^{n} (Y_e[i] - Y[i])^2 \qquad (5.1)$$

Where

ϕ = sum of square of the difference,

Y_e = experimental data point,

Y = model calculated data point, and

n = number of points.

The values of what are thought to be the three critical parameters (τ, S_0, and D_0) were manually changed and by trail-and –error observation, the smallest values for ϕ, the sum of square of the differences were obtained. Using the values of the three parameters that reduced the ϕ, the hydrogen flux values were predicted and compared to data (9) at two other temperatures (900°F and 1300°F). The same values of τ, S_0, and D_0 were used at all three temperatures. The hydrogen flux values were also calculated for a diffusion-limiting permeation. Figure 16 shows the comparison of flux of hydrogen gas versus feed side hydrogen partial pressure for Pd/Al_2O_3 composite membrane at temperature of 1100^0F (866.48K). The dashed line is our model calculation and the solid line indicates the diffusion-limited flux predicted under conditions of interfacial equilibrium (Equations (3.18), (3.34), and (3.42)). The experimental flux at hydrogen partial pressure below 2 atm was slightly higher than the model predicted flux and diffusion limited flux but the model predicted flux was a fairly good fit for the experimental flux at hydrogen partial pressure above 2 atm. Similarly, in Figure 17 the model predicted flux was a fairly good fit for the experimental flux at the temperature of 1300^0F (977.59K). In Figure 18, the model predicted flux was not a good fit for the experimental flux at the temperature of 900^0F (755.37K). This can be attributed to the fact that there can be considerable changes taking place in the pore structure of the palladium specimens after several cycles of adsorption and desorption of hydrogen. In literature it is claimed that during adsorption/desorption, $\alpha \rightarrow \beta$ phase and $\beta \rightarrow \alpha$ phase transformations in palladium do occur over the time (19).

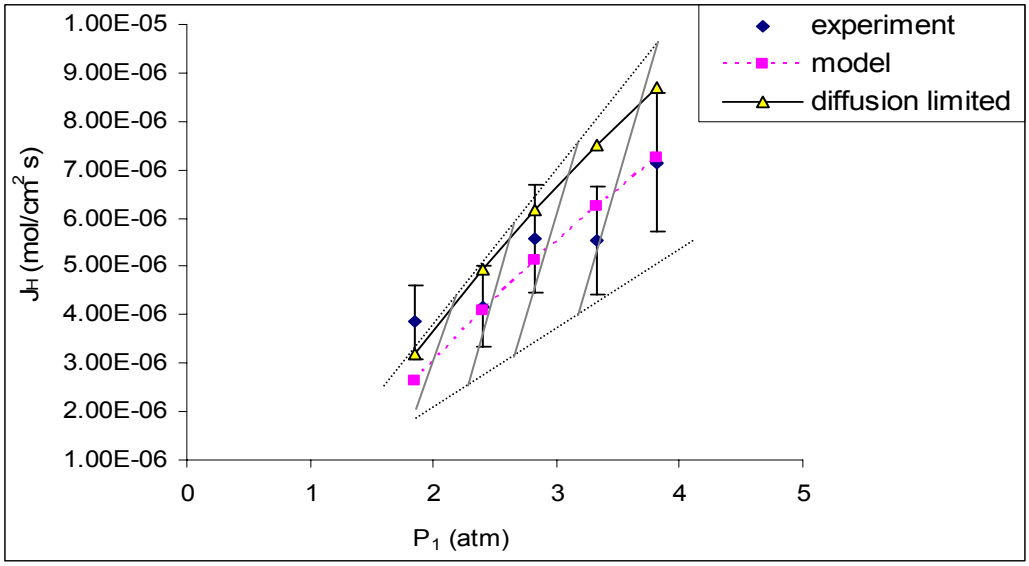

Figure 16 Plots of atomic hydrogen flux, J_H, versus feed side hydrogen gas partial pressure, P_1, for Pd/Al_2O_3 composite membrane at temperature of 1100^0F (866.48K).

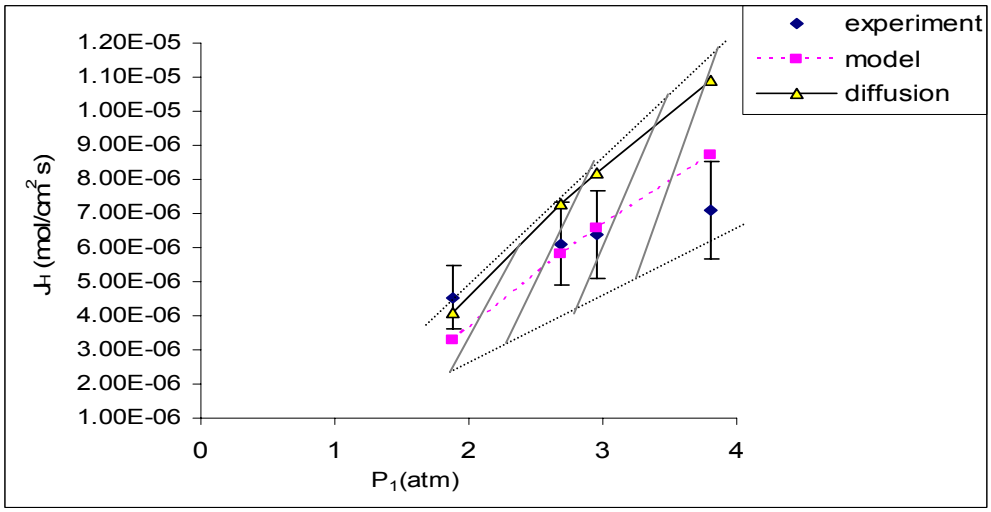

Figure 17 Plots of atomic hydrogen flux, J_H, versus feed side hydrogen gas partial pressure, P_1, for Pd/Al_2O_3 composite membrane at temperature of 1300^0F (977.59K).

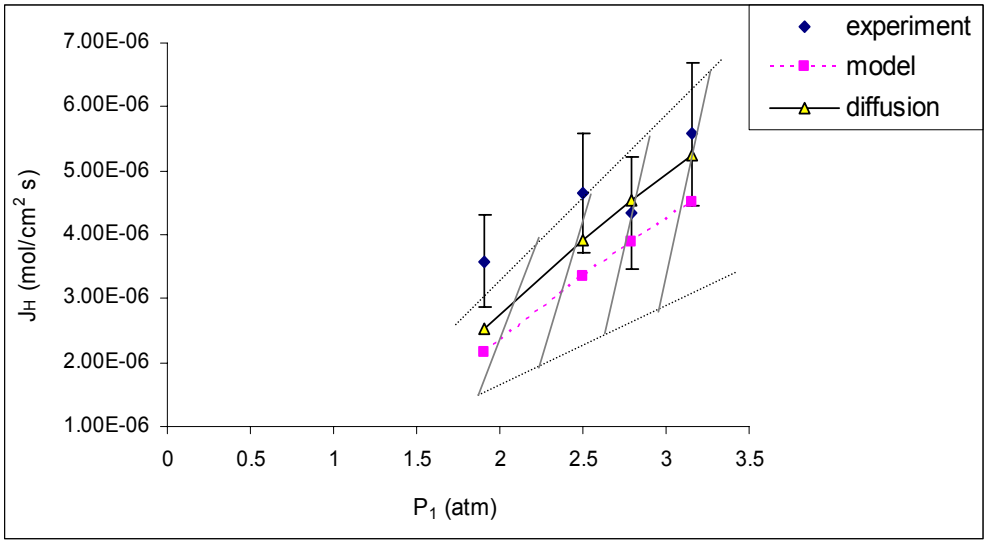

Figure 18 Plots of atomic hydrogen flux, J_H, versus feed side hydrogen gas partial pressure, P_1, for Pd/Al_2O_3 composite membrane at temperature of 900^0F (755.37K).

There have also been a number of reports of the observation of microscopic changes taking place on the surfaces of palladium specimens following the adsorption of hydrogen leading to cracks in the Pd film. This may have happened in the experimental work at UTSI too (9). In Figures 16, 17 and 18, the region shown by the cross hatched lines show that within ± 30% all the experimental data can be very well simulated by our data. Even at 900^0F, the match between the predicted data and actual data is acceptable; most of the experimental values are within 30% of the model predicted data and have at least the same order of magnitude. Further attempts to improve the match with the experimental data at 900^0F and 1300^0F were not made, because at this point we were only interested in developing a mechanistic model that can reasonably simulate the transport steps taking place during hydrogen permeation through Pd/alumina composite membrane.

5.3 Rate Limiting Flux

To determine the rate limiting step, calculations were carried out under the hypothetical situation where only one step is the slowest step and the rate limiting step and others are much faster. Figures 19, 20 and 21 show plots of predicted atomic hydrogen flux rate predicted from our model equations for each forward rate process under such hypothetical condition. In this situation, the mass transfer step with the lowest rate limiting flux at any temperature would be the overall rate controlling step at that temperature. From Figures 19, 20 and 21, atomic H diffusion through the palladium layer, and the pore diffusion of H through the porous support, was found to be the greatest rate limiting fluxes. Table 4 shows a summary of the individual mass transfer steps and the equations involved. The model calculations indicate that the atomic diffusion in the palladium layer and the pore diffusion in the porous alumina support seem to have the greatest influence on the H permeation rate since both of them provide the rate limiting flux. The actual overall rate of permeation can also be limited by a combination of the rate of atomic diffusion in the dense Pd layer and the pore diffusion in the porous alumina support. Diffusion limited fluxes have been reported in most permeation literature data (2, 3, 7, 20, 23, 32, 33). The significance of mass transfer resistance associated with the diffusion through the porous support has also been reported (2, 35, 36). The mass transfer step with the greatest influence on the hydrogen permeation is discussed next by estimating the individual transport resistances.

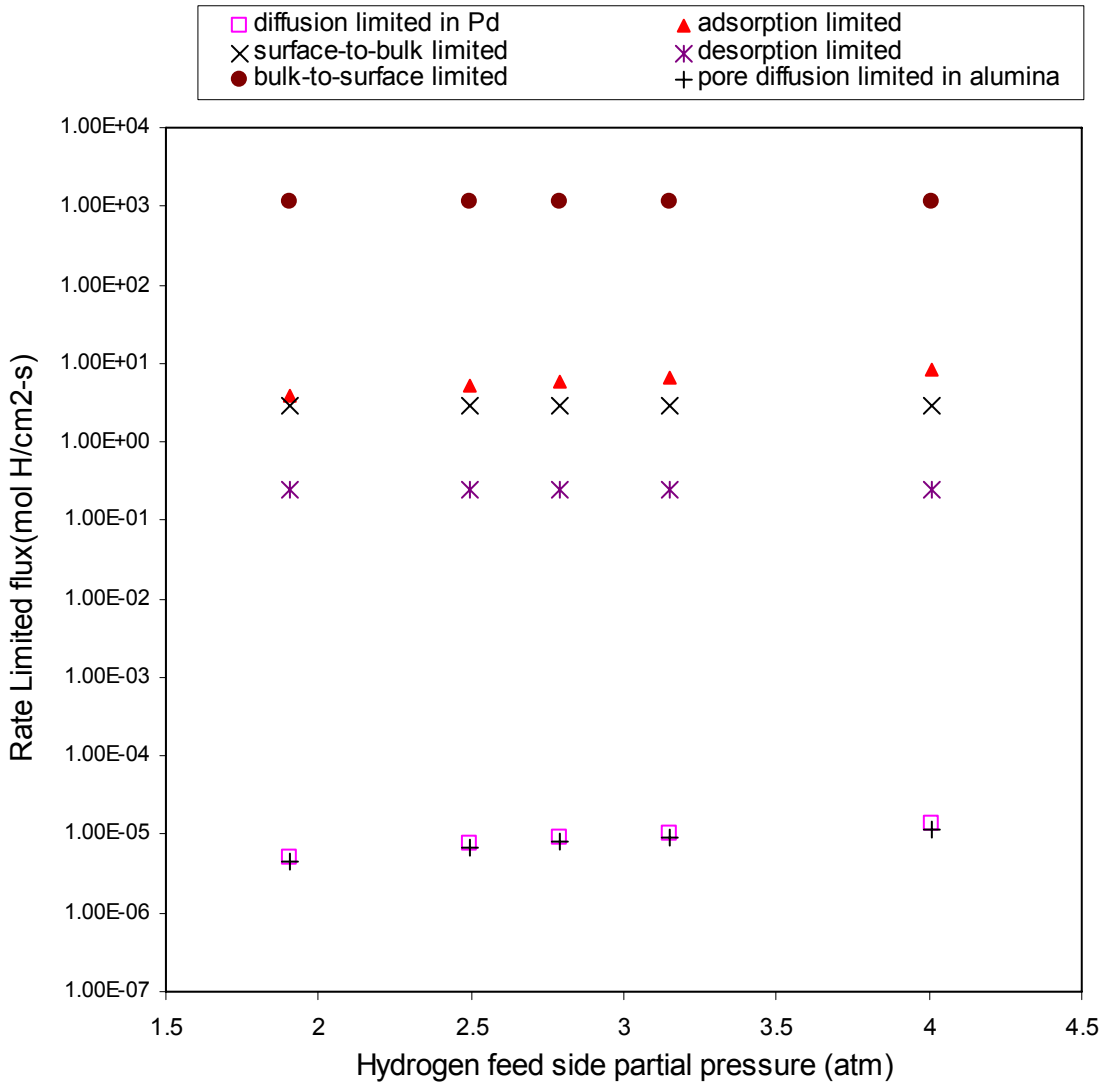

Figure 19 Plots showing the hypothetical flux predicted for conditions when various mass transfer steps are the rate limiting step at 900^{0}F (755.37K).

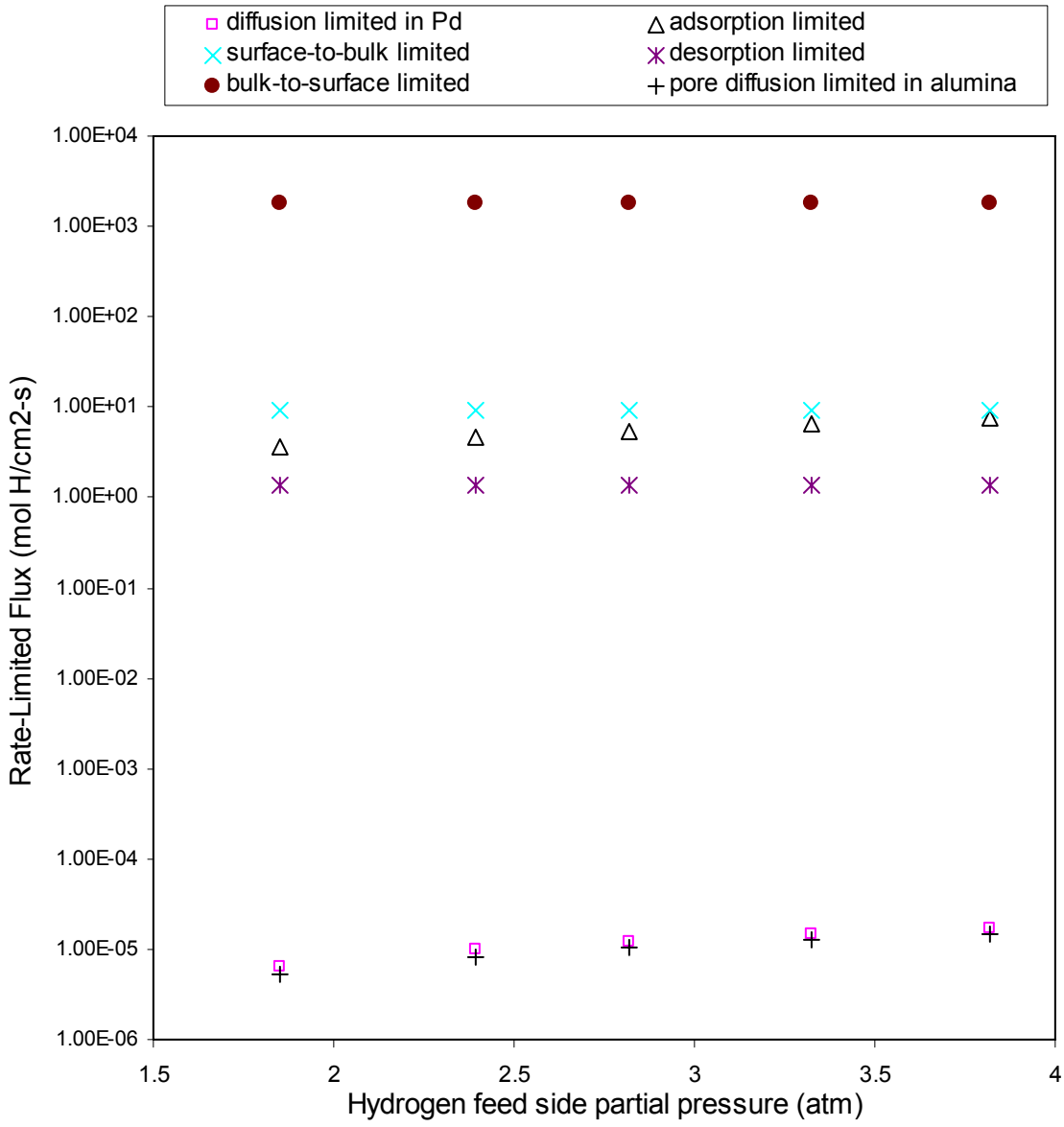

Figure 20 Plots showing the hypothetical flux predicted for conditions when various mass transfer steps are the rate limiting step at 1100^{0}F (866.48K).

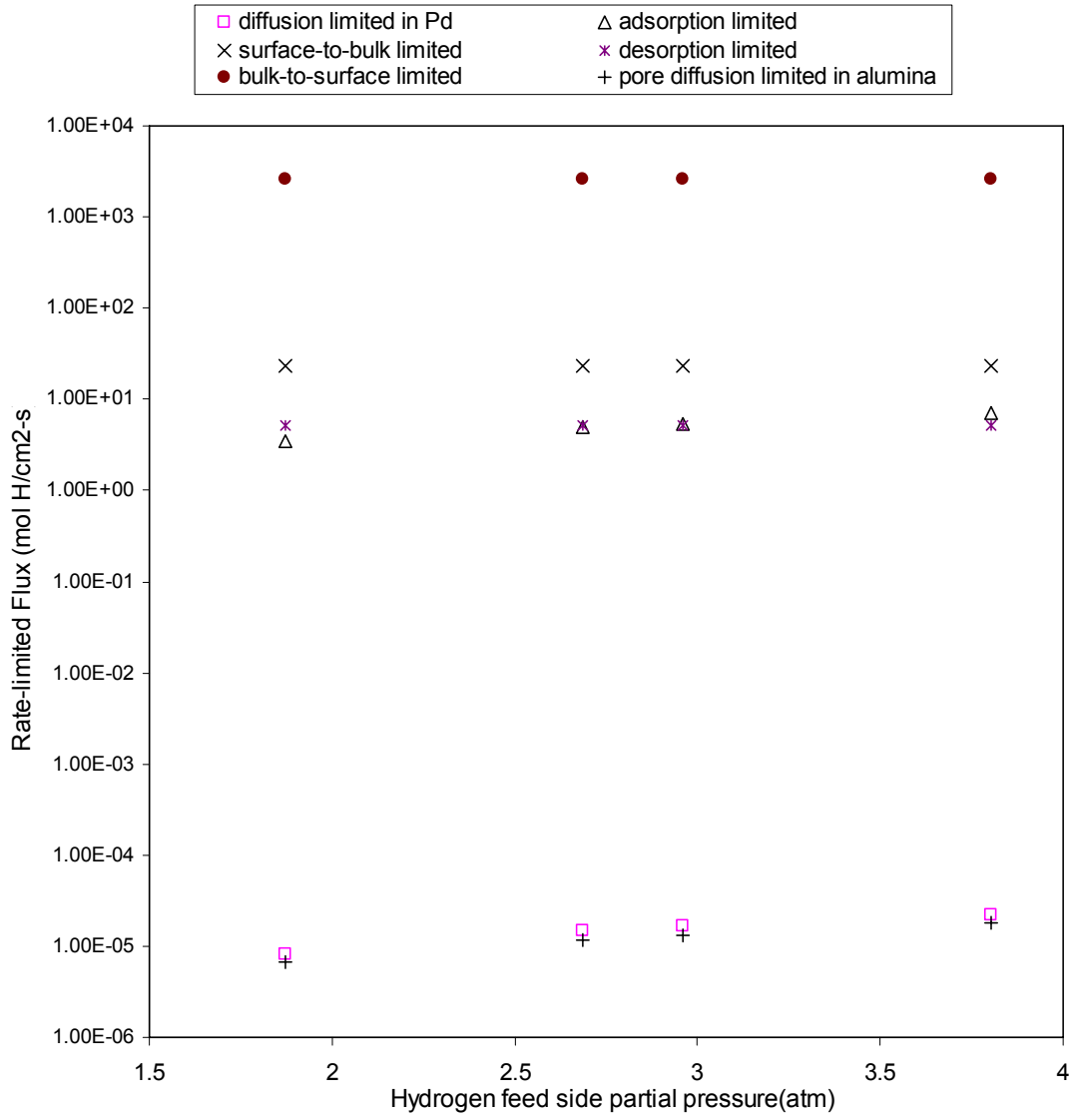

Figure 21 Plots showing the hypothetical flux predicted for conditions when various mass transfer steps are the rate limiting step at 1300^{0}F (977.59K).

Table 4 Summary of the individual rate limiting mass transfer steps and the equations involved.

Rate limiting mass transfer step	Equation
Adsorption rate	Equation (3.7) with $S(\theta)$=1
Surface-to-bulk Pd metal transport rate	Equation (3.14) with θ_1=1 and X_1 =0
Atomic diffusion in Pd rate	Equation (3.18) with X_{1s} and X_{2s} given by Sievert's law
Bulk Pd metal-to-surface rate	(3.20) with X_2 =1 and θ_2=0
Desorption rate	Equation (3.28) with θ_2=1
Pore diffusion rate in the alumina support	Equation (3.48)

5.4 Estimation of Resistance to Individual Mass Transfer Step

An electrical analogy based on resistance, for permeation in composite membrane was developed by Henis and Tripodi (51). According to this model, the permeation behavior of gas through a composite membrane is analogous to the flow of electricity through a series-parallel array of resistors. In Figure 22, R_s denotes the transport resistance in the alumina support, and R_{Pd} is the transport resistance in the dense palladium layer. At steady state, the overall transport resistance, R_{tot}, equals the sum of the Pd layer and the porous alumina support as given by (2):

$$R_{tot} = \frac{1}{F_P} \qquad (5.1)$$

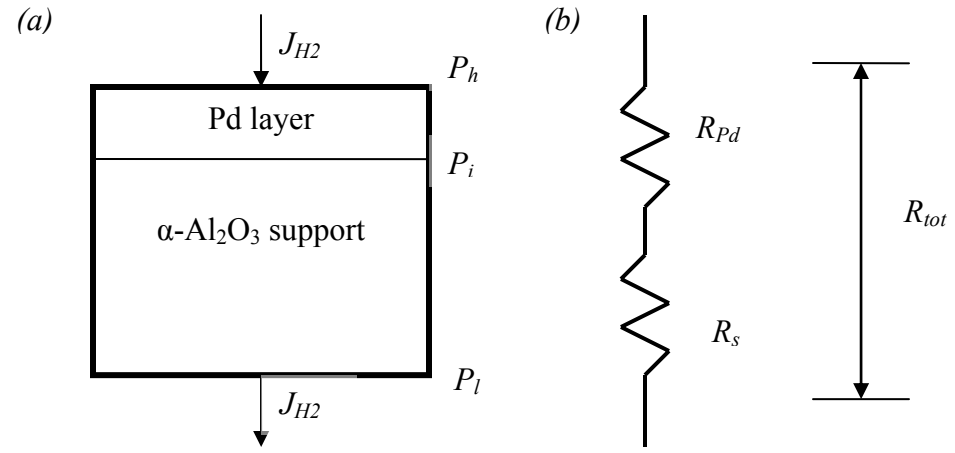

Figure 22 (a) Simplified schematic structure of the Pd/alumina composite membrane, (b) Schematic representation of resistance model for composite membrane (taken from ref. 2).

$$R_{tot} = R_s + R_{Pd} \tag{5.2}$$

Where

$$R_s = \frac{P_i - P_l}{J_{H2}}$$

$$= \frac{RT(C_i - C_l)}{J_{H2}} \tag{5.3}$$

Similarly,

$$R_{Pd} = \frac{RT(C_h - C_i)}{J_{H2}} \tag{5.4}$$

The interfacial pressure, P_i, is determined from the model calculation, R_s and R_{Pd} can then be estimated from Equations (5.3) and (5.4), respectively. In the resulting concentration profiles shown in Figures 23, 24, and 25, the layer with the highest concentration gradient (slope) provides the greatest mass transfer resistance to the permeation process. The x-axis in Figures 23, 24 and 25 were not drawn to scale. At temperatures 900^0F (755.37K), 1100^0F (866.48K) and 1300^0F (977.59K), the steepest slope was found to exist in the palladium layer, and therefore, the relative mass transfer resistance in the palladium layer would influence the permeation process the most. This is consistent with the literature, where atomic (bulk) diffusion in the palladium layer was reported to be the rate limiting (slowest) step (3, 7, 20, 23, 32, 33).

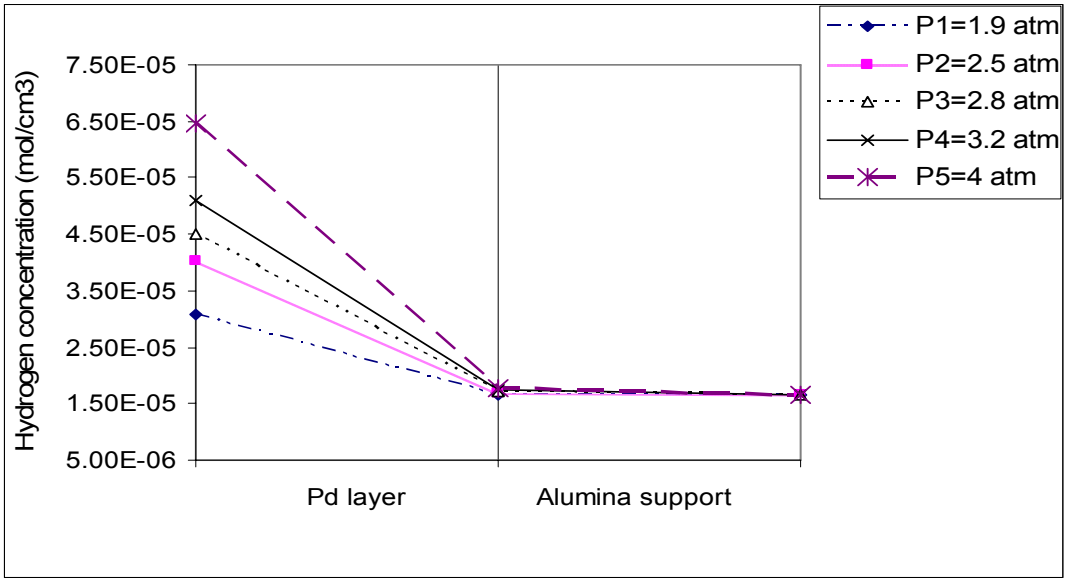

Figure 23 Concentration profiles in the Pd and alumina layers at different hydrogen partial pressures and 900^0F.

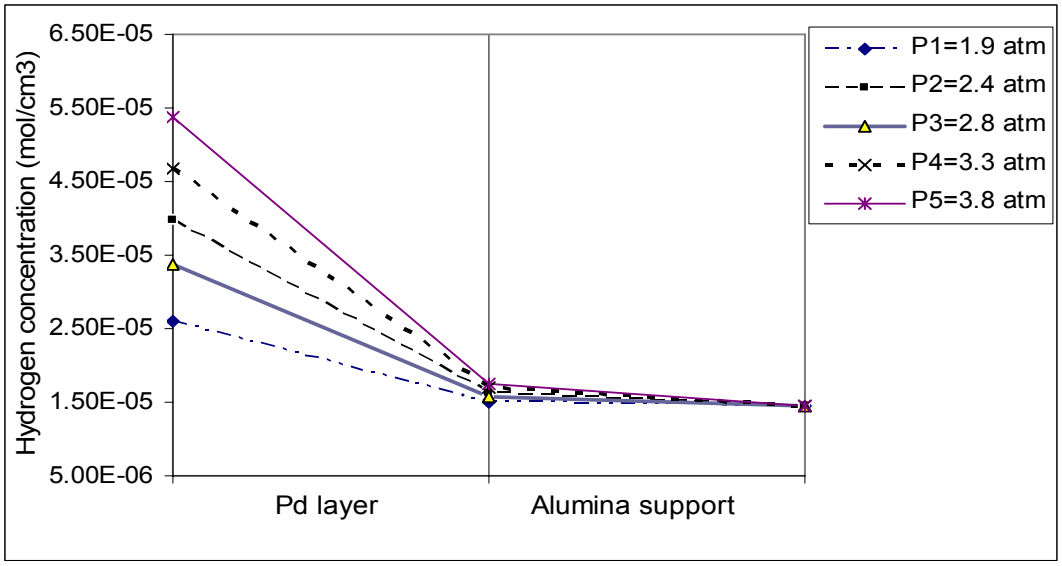

Figure 24 Concentration profiles in the Pd and alumina layers at different hydrogen partial pressures and 1100^{0}F.

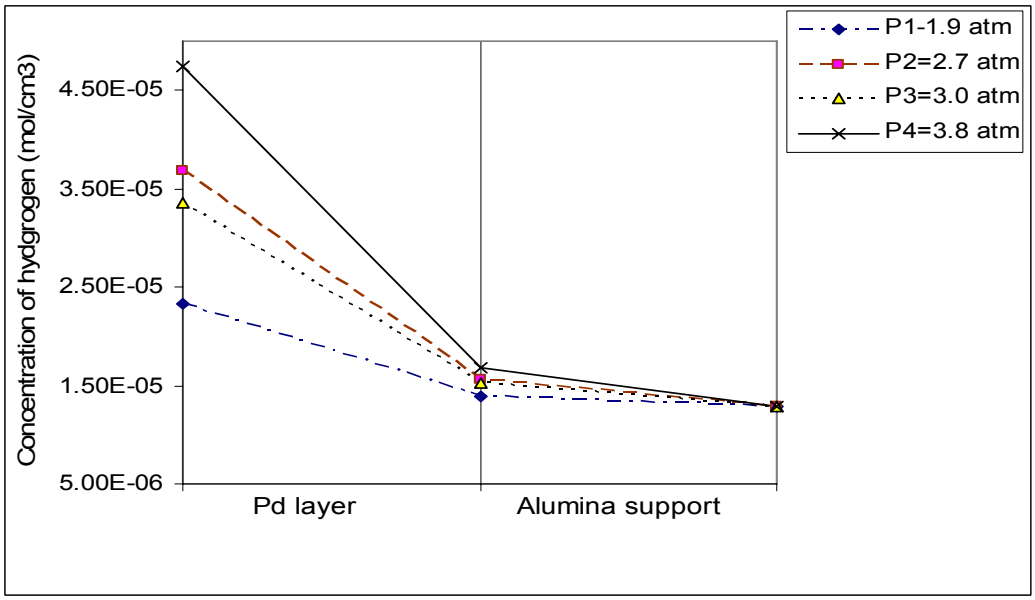

Figure 25 Concentration profiles in the Pd and alumina layers at different hydrogen partial pressures and 1300^{0}F.

The relative mass transfer resistances in the two layers, R_{Pd}/R_{tot} (palladium layer) and R_s/R_{tot} (porous alumina support layer) may be calculated from equations (5.2), (5.3) and (5.4). The results of mass transfer resistances at different temperature are given in Tables 5, 6 and 7. At 900^0F, 93% of the mass transfer resistance seems to be coming from the palladium layer and 7% from the porous alumina support. At 1100^0F, 90.2% of the mass transfer resistance is from the palladium layer and 9.8% from the porous alumina support. At 1300^0F, 87.3% of the mass transfer resistance is from the palladium layer and 12.7% from the porous alumina support. The mass transfer resistance from the palladium layer decreased with temperature, this maybe attributed to the fact that grain boundary diffusion was dominant diffusion mechanism at higher temperature when compared to the bulk diffusion. It can also been seen in Figures 23, 24 and 25 that the mass transfer resistance in the palladium layer increased as the hydrogen feed side partial pressure increased. This may be attributed to the fact that the mass transfer resistance is proportional to hydrogen partial pressure gradient as shown in equation (5.3). The driving force in the palladium membrane is the gradient of pressure.

Table 5 Calculated mass transfer resistances for Pd/Al_2O_3 membrane at 900^0F.

P_1(atm) (feed side)	Resistance in Pd (R_{Pd}) (mol/cm^2.s.atm)	Resistance in Al_2O_2 (R_s) (mol/cm^2.s.atm)	Total Resist. (R_{tot}) (mol/cm^2.s.atm)	R_{pd}/R_{tot} (%)	R_s/R_{tot} (%)
1.9060	3.71E+05	3.17E+04	4.03E+05	92.1	7.9
2.4972	4.05E+05	3.16E+04	4.37E+05	92.8	7.2
2.7919	4.20E+05	3.16E+04	4.52E+05	93.0	7.0
3.1533	4.38E+05	3.16E+04	4.70E+05	93.3	6.7
4.0091	4.77E+05	3.15E+04	5.09E+05	93.8	6.2
			Average	93.0	7.0

Table 6 Calculated mass transfer resistances for Pd/Al_2O_3 membrane at 1100^0F.

P_1(atm) (feed side)	Resistance in Pd (R_{pd}) (mol/cm^2.s.atm)	Resistance in Al_2O_2 (R_s) (mol/cm^2.s.atm)	Total Resist. (R_{tot}) (mol/cm^2.s.atm)	R_{pd}/R_{tot} (%)	R_s/R_{tot} (%)
1.8506	2.74E+05	3.41E+04	3.08E+05	88.9	11.1
2.3953	2.98E+05	3.40E+04	3.32E+05	89.8	10.2
2.8211	3.15E+05	3.40E+04	3.49E+05	90.3	9.7
3.3250	3.34E+05	3.39E+04	3.68E+05	90.8	9.2
3.8196	3.51E+05	3.39E+04	3.85E+05	91.2	8.8
			Average	90.2	9.8

Table 7 Calculated mass transfer resistances for Pd/Al_2O_3 membrane at 1300^0F.

P_1(atm) (feed side)	Resistance in Pd (R_{pd}) (mol/cm^2.s.atm)	Resistance in Al_2O_2 (R_s) (mol/cm^2.s.atm)	Total Resist. (R_{tot}) (mol/cm^2.s.atm)	R_{pd}/R_{tot} (%)	R_s/R_{tot} (%)
1.8734	2.20E+05	3.64E+04	2.56E+05	85.8	14.2
2.6870	2.48E+05	3.62E+04	2.84E+05	87.3	12.7
2.9599	2.57E+05	3.62E+04	2.93E+05	87.6	12.4
3.8039	2.81E+05	3.61E+04	3.17E+05	88.6	11.4
			Average	87.3	12.7

5.5 Application of the Present Model Results to Define Membrane Design for DOE Goal

The DOE commercial target for membrane separation is to achieve hydrogen fluxes in excess of 60 scfh/ft^2 (~30 cc/cm^2-min). Our model was used to come up with the necessary conditions to achieve hydrogen flux values that DOE has set as a goal. This is illustrated in Figure 26. Hydrogen flux values were plotted as function of Pd layer thickness while also varying the alumina layer thickness and the porosity of the alumina layer.

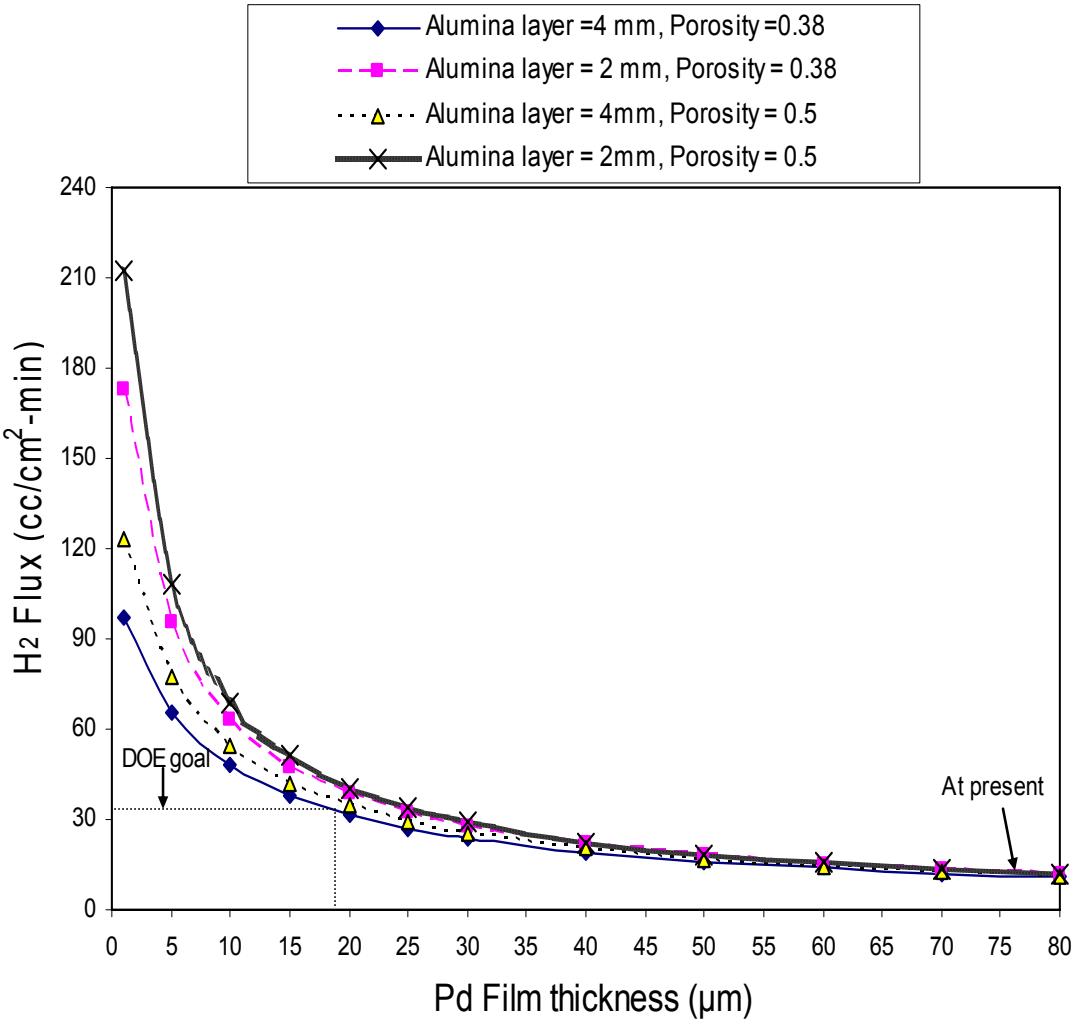

Figure 26 Plots of hydrogen flux verses Pd film thickness at 1300^{0}F and hydrogen feed side partial pressure of 3.8 atm.

Fluxes in excess of 60 scfh/ft2 (~30 cc/cm2-min) can be achieved by reducing the thickness of the Pd layer to about 18 μm, while keeping alumina layer specification the same. This can also be achieved by reducing the Pd layer to about 20 μm and decreasing the thickness of the alumina layer to about 2 mm or increasing it's porosity to about 0.5.

6. CONCLUSIONS AND RECOMMENDATIONS

6.1 Conclusions

A mechanistic model of hydrogen permeation in palladium/alumina composite membrane has been developed taking into account the adsorption/desorption kinetics in thin Pd membrane and the permeation flow in the porous alumina support. The necessary parameters used in the kinetics of H_2 adsorption/desorption at the palladium surface were estimated from the surface science literature and related membrane literature. Knudsen diffusion and viscous flow (Hagen-Poisuielle type) were used to model permeation behavior in the porous alumina support. In our study, the model developed was found to be in agreement with the literature and was able to satisfactorily predict experimentally observed flux values obtained at UTSI on a new type of palladium composite membrane. A simplified resistance model was also employed to analyze the permeation behavior of hydrogen through the palladium/alumina composite membrane to identify the major resistances to the mass transfer.

The model predicted flux values provided a good fit to the experimental flux values at 1100^0F and1300^0F, and satisfactory fit at 900^0F. This slightly poor fit at 900^0F was attributed to possible microscopic (pore size and pore size distribution) changes and structural changes taking place in the UTSI palladium specimens after several tests (heating and cooling cycles of the membrane). Our calculations indicate that bulk

diffusion through the Pd layer was probably the rate limiting step and is consistent with the literature for membrane thickness greater than 10 μm. Mass transfer resistance in the Pd layer was found to have the greatest influence on the permeation process and it decreased as the temperature increased from 900^0F to 1300^0F. A slightly lower but still significant mass transfer resistance due to the porous alumina support was also observed from the model calculations and it also increased with the temperature. Our model calculations also indicated that by reducing the thickness of the Pd layer to about 18 μm, the DOE goal of 60 scfh/ft^2 hydrogen flux can be achieved. This can also be achieved by reducing the thickness of the Pd layer to about 20 μm and reducing the thickness of the alumina layer to about 2mm or increasing it's porosity to about 50%.

6.2 Recommendations

Our model calculations indicate that atomic diffusion through the Pd layer is most likely the rate limiting step in the hydrogen permeation through Pd/Al_2O_3 composite membrane. Since permeation is inversely proportional to the membrane thickness, reducing the thickness of the membrane will increase the permeation flux. Also, since the resistance of the support to the hydrogen flux cannot be neglected, increasing the pore size and decreasing the thickness of the support would also increase the hydrogen permeation flux. Hence it is recommended that in future study, Pd films of about 20 μm thick should be deposited onto a suitable alumina support of about 2 mm thickness and porosity of about 50%, to get the fluxes in excess 60 scfh/ft^2 (~30 cc/cm^2-min) considered to be necessary for the commercial applications in hydrogen fuel cells.

The substitution of pure palladium with certain palladium alloys which do not seem to undergo microscopic changes and changes in shape of the membrane specimen (disc size) and can also permit even higher rates of permeation of hydrogen under comparable conditions should be considered. Examples of such alloys of Pd are Pd-Ag, Pd-Cu and Pd-Ru. Alloying Pd with Ag will increase hydrogen permeability and the mechanical strength of the membrane. Further research in the effects of micro-structural behavior on the rate of permeation in Pd or Pd alloy as a function of several cycling should be carried out to establish the effect of microscopic changes on the permeation process. More work on the effect of grain boundary on the rate of diffusion should be done.

REFERENCES

1. Morreale, B. D., Ciocco, M.V., Enick , R. M , Morsi , B. I. ,Howarda, B. H., Cugini , A. V. , Rothenberger, K. S., "The permeability of hydrogen in bulk palladium at elevated temperatures and pressures," J. Membrane Sci, 212, p 87, 2003.
2. Huang, T. C., Wie, M. C., and Chen, H. I., "Permeation of hydrogen through palladium/alumina composite membrane," Sep. Sci. Technol., 36(2), p 199, 2001.
3. Konno, M., Shindo, M., Sugawara, S. and Saito, S., "A composite palladium and porous alumina oxide membrane for hydrogen gas separation," J. Membrane Sci, 37, p 193, 1998.
4. Li, Z. Y., Maeda, H., Kusakabe, K., Morooka, S., Anzai, H., and Akiyama, S., "Preparation of palladium-silver alloy membranes for hydrogen separation by the spray pyrolysis method," J. Membrane Sci., 78, p 247, 1993.
5. Yan, S., Maeda, H., Kusakabe, K., and Morooka, S., "Thin palladium films formed in support pores by metal-organic chemical vapor deposition method and application to hydrogen separation," Ind. Eng. Chem. Res., 33, p 616, 1994.
6. Shu, J., Grandjean, B. P. A., Van Neste, A., and Kiliaguine, S.," Catalytic palladium-based membrane reactors: a review," Canadian J. Chem Eng. 69, p 1036, 1991.
7. Ward, T. L., and Dao, T., "Model of hydrogen permeation behavior in palladium membranes," J. Membrane Sci., 153, p 211, 1999.
8. Huang, T. C., and Chen, H. I., "A study on the preparation and gas permeation of porous alumina support," Sep. Sci. Technology, 30, p 2189, 1995.
9. Singh, B. K., "Bench scale evaluation of dense ceramic membranes for production of high purity hydrogen from gasification," Masters Thesis - University of Tennessee, 2005.

10. Souleimanova, R. S., Mukasyan, S. A., and Varma, A., "Pd membranes formed by electroless plating with osmosis: hydrogen permeation studies," AIChE J., 48, p 262, 2002.
11. Behm, R. J., Christmann, K., and Ertl G., "Adsorption of hydrogen on Pd (100)," Surface Science, 99, p 320, 1980.
12. Conrad, H., Ertl G., and Latta, E. E., "Adsorption of hydrogen on palladium single crystal surfaces," Surface Science, 41, p 435, 1974.
13. Burggraaf, A. J., "Important characteristics of inorganic membranes," in: Burggraaf, A. J. and Cot L. (Eds), Fundamentals of Inorganic Membrane Science and Technology, Elsevier, Amsterdam, p 21, 1996.
14. Jose, G. S. M., and Tsotsis T. T., "Catalytic membranes and membrane reactors," Wiley-VCH, Verlag GmbH, Weinheim, 2002.
15. Lin, Y. S., and Xomeritakis, G., "Fabrication of a thin palladium membrane supported in a porous ceramic substrate by chemical vapor deposition," Journal of Membrane Science, 120, p 261, 1996.
16. Feurer, E., and Suhr, H., "Thin palladium films prepared by metal organic plasma enhanced CVD," Thin Solid Films, 157, p 81, 1988.
17. Uemiya, S., Matsuda, T., and Kikuchi, E., "Hydrogen permeable palladium-silver alloy membrane supported on porous ceramics," J. Membrane Sci., 56, p 315, 1991.
18. Shu, J., Grandjean, B. P. A., Ghali, E., and Kaliaguine, S., " Simultaneous deposition of Pd and Ag on porous stainless steel by electroless plating," J. Membrane Sci., 77, p 181, 1993.
19. Lewis, F. A., "The palladium hydrogen system," Academic Press, London, 1967.

20. Buxbaum, R. E., and Kinney, A. B., "Hydrogen transport through tubular membranes of palladium-coated tantalum and niobium," Ind. Eng. Chem. Res., 35, p 530, 1996.
21. Gabrielle, C., Grand, P. P., Lasia, A., and Perrot, H., "Investigation of hydrogen adsorption-absorption into thin palladium films," J. of the Electrochemical Society, 151, p A1925, 2004.
22. Volkl, J., and Alefeld, G., "Hydrogen diffusion in metals," in: Nowick A. S., Burton J. J. (Eds), Diffusion in solids, recent developments, Academic Press, New York, p 231, 1975.
23. Holleck, G. L., "Diffusion and solubility of hydrogen in palladium and palladium-silver alloys," J. Phys. Chem., 74, p 503, 1970.
24. Birnbaum, H. K., and Weat, C. A., "Diffusion of hydrogen in metals," Ber Bunsenges. Physik. Chem., 76, p 806, 1972.
25. Nagamoto, H., and Inoue, H., "Sorption and desorption of hydrogen on palldiun sheet", Nippon Kagaku Kaishi, 9, p 1264, 1977
26. Kay, B. D., Penden, C. H. F., and Goodman, D. W., "Kinetics of hydrogen absorption by Pd (110)", Phys. Rev. B 34, p 817, 1986.
27. Volkl, J., and Alefeld, G., "Diffusion of hydrogen in metals," in: Alefeld, G., Volkl, J. (Eds), Hydrogen in metals, Vol I, Topics in Applied Physics, 28, p 321, 1978.
28. Gryaznov, V. M., "Hydrogen permeable palladium membrane catalysts. An aid to the efficient production of ultra pure chemical and pharmaceuticals," Platinum Met. Rev., 30, p 68, 1986.
29. Itoh, N., "A membrane reactor using palladium," *AIChE J.,* 33, p 1576, 1987.

30. Uemiya, S., Sato, N., Ando, H. and Kikuchi, E., "The water gas shift reaction assisted by a palladium membrane reactor," Ind. Eng. Chem. Res., 30, p 585, 1991.
31. Collins, J. P., and Way, J. D., "Preparation and characterization of a composite palladium-ceramic membrane," Ind. Eng. Chem. Res., 32, p 3006, 1993.
32. Hurlbert, R. C., and Konecny, J. O., "Diffusion of hydrogen through palladium," J. Chemical Physics, 34, p 655, 1961.
33. Uemiya, S., Sato, N., Ando, H., Kude, Y., Atsuda, T. and Kikuchi, E., "Separation of hydrogen through palladium thin film supported on a porous glass tube," J. Membrane Sci., 56, p 303, 1991.
34. Ali-Khan, I., Dietz, K. J., Waelbroeck, F. G., and Woenhold, P., "The rate of hydrogen release out of clean metallic surfaces," J. Nuclear Mater. 76, p 337, 1978.
35. Huang, T. C., Wie, M. C., and Chen, H. I., "A study of hydrogen transport properties of palladium/alumina composite membrane," Chem. Eng. Comm., 189, p 1340, 2002.
36. Burggraaf, A. J., "Transport and separation properties of membranes with gases and vapors," in: Burggraaf, A. J. and Cot L. (Eds), Fundamentals of Inorganic Membrane Science and Technology, Elsevier, Amsterdam, p 331, 1996.
37. Pick, M. A., "The kinetics of hydrogen absorption-desorption," in: Bambakidis, G. (Ed.), Metal Hydrides, Plenum Press, New York, p 329, 1981.
38. Hines, A. L., and Maddox, R. L., "Mass transfer, fundamentals and applications," Prentice-Hall, New Jersey, 1985.
39. Ash, R., and Barrer, R. M., "Permeation of hydrogen through metals," Phil. Mag., 4, p 1197, 1959.

40. King, D. A., and Wells, M. G., "Reaction mechanism in chemisorption kinetics: nitrogen on the {1 0 0} plane of tungsten," Proc. R. Soc. London, Ser. A, 339, p 245, 1974.
41. Lynch, J. F., and Flanagan, T. B., "An investigation of the dynamic equilibrium between chemisorbed and absorbed hydrogen in the palladium/hydrogen system," J. Phys. Chem. 77, p 2628, 1973.
42. Borg, R. J., and Dienes, G. J., "An introduction to solid state diffusion," Academic Press, San Diego, 1988.
43. Wert, C., and Zener, C., "Interstitial atomic diffusion coefficients," Phys. Rev., 76, p 1169, 1949.
44. Flanagan, T. B., and Oates, W. A., "The palladium-hydrogen system," Annu. Rev. Mater. Sci., 21, p 269, 1991.
45. Flanagan, T .B., and Oates, W. A., "Thermodynamics of metal/hydrogen systems," Ber. Bunsenges. Physik. Chem. 76, p 706, 1972.
46. Fowler, R., and Guggenheim, E. A., "Statistical Thermodynamics," Cambridge University Press, London, 1965.
47. Kesting, R. E., and Fritzsche, A. K., "Polymeric gas separation membranes," John Wiley & Sons, Inc., New York, 1993.
48. Sakamoto, F., Kinari, Y., Chen, F. L., and Sakamoto, Y., "Hydrogen permeation through palladium alloy membranes in mixture of gases of 10% nitrogen and ammonia in the hydrogen," Int. J. Hydrogen Energy, 22, p 369, 1997.

49. Chen, F. L., Kinari, Y., Nakayam, Y., and Sakamoto, Y., "Hydrogen permeation through palladium-based alloy membranes in mixture of gases of 10% methane and ethylene in the hydrogen," Int. J. Hydrogen Energy, 21, p 555, 1996.
50. Clouse, R. L., "The mathematical modeling and validation of gas flow processes in large industrial facilities," Ph. D Dissertation-University of Tennessee, p 98, 1990.
51. Lalwani, C. S., "Verification and validation of simulation in social sciences," Proceedings of the 1982 Summer Computer Simulation Conference, July 1982.
52. Sargent, R. G., "Verification and validation of simulation models," in: Medeiros, D. J., Watson, E. F., Carson, J. S., and Manivannan, M. S. (eds), Proceedings of the 1998 Winter Simulation Conference, 1998.
53. Henis, J. M., and Tripodi, M. K., "Composite hollow fiber membranes for gas separation: the resistance model approach," J. Membrane Sci., 8, p 233, 1981.
54. Bird, R. B., Stewart, W. E., and Lightfoot, E. N., "Transport phenomena," John Wiley & Sons, Inc., New York, 2nd Edition, 2002.
55. Behm, R. J., Penka, V., Cattania, M. G., Christmann, K., and Ertl, G., "Evidence of "subsurface" hydrogen on Pd (1 0 0): an intermediate between chemisorbed and dissolved species," J. Chem. Phys., 78, p 7482, 1983.
56. Amandusson, H., Ekedahl, L. G., and Dannetum, H., "Hydrogen permeation through surface modified Pd and Pd-Ag membrane," J. Membrane Sci., 193, p 35, 2001.
57. Perry, R. H., and Green, D. W., 'Perry's Chemical Engineers' Handbook," 7th Edition, 1997.

APPENDICES

Appendix I-Computer Programs

I1-Program for Model Calculation


```
(*PROGRAM FOR MODEL CALCULATION*)
(*INPUT VARIABLES*)
P11 = 1.850607493;
(*hydrogen gas partial pressure
 in the feed side (atm)*)
P12 = 2.821064187;   (*hydrogen gas partial
 pressure in the feed side (atm)*)
P13 = 2.395280213;    (*hydrogen gas
 partial pressure in the feed side (atm)*)
P14 = 3.324957416;   (*hydrogen gas partial
 pressure in the feed side (atm)*)
P15 = 3.819561877;     (*hydrogen gas
 partial pressure in the feed side (atm)*)
P2 = 1.033;          (*hydrogen gas partial
 pressure in the permeate side (atm)*)
T = 866.483;         (*reactor temperature*)

(*OUTPUT VARIABLES*)
(*Ø1,Ø2; surface coverage on the
 feed side and permeate side respectively
 (H/Pd atom ratio on the surface)*)
(*X1,X2 ; H/Pd ratio in the bulk metal
 adjacent to high and low partial
 pressure surfaces respectively*)
(*C2i; gas phase interface hydrogen
 concentration (mol/cm^3)*)
(*J1; H atom flux (mol H/cm^2 s)*)

(*CONSTANTS*)
M = 2.016;
(*molecular weight of hydrogen *)
R = 82.0578;
(* gas constant (cm^3 atm/g-mol.K)*)
C1 = P11 / (R * T);
(* gas phase hydrogen concentration
 in the feed side (mol/cm^3)*)
C2 = P2 / (R * T);     (* gas phase hydrogen
 concentration in the permeate side (mol/cm^3)*)
Ed = 10;              (* H atom desorption
```

```
 activation energy (kcal/mol-H)*)
Ea = 13.45;
(* activation energy for surface-to-
 bulk metal transition (kcal/mol-H)*)
Eb = 5.45;
(* activation energy for H atom metal-
 to-surface transition (kcal/mol-H)*)
Edi = 5.45;          (* activation energy
 for H atom diffusion in Pd (kcal/mol-H)*)
k0 = 4.8 * 10^21;
(* desorption rate constant pre-
 exponential factor (cm^3/mol-Hs)*)
ß0 = 6.8 * 10^13;     (* rate constant pre-
 exponential factor for metal-to-
 surface transition (cm^3/mol-Hs)*)
D0 = 3.3 * 10^-3;
(*pre-exponential factor for diffusion
  coefficeint for H atoms in Pd (cm^2/s)*)
Nb = 0.113;          (*bulk metal Pd
 atom concentration (mol Pd/cm^3) *)
Ns = 2.8 * 10^-9;      (*Pd atom surface
 concentration (mol Pd atoms/cm^2)*)
w = 0.5;            (*pairwise interaction
 energy between H atoms on surface (kcal/mol)*)
K = 0.05;           (*constant used in
 sticking model (dimensionless)*)
k = R / (6.02214 * 10^23); (*Boltsmann' s constant*)
S0 = 0.95;
(*initial sticking coefficient (dimensionless)*)
z = 4;
(*number of nearest neighbors*)
DZ = 77 * 10^-4;       (*membrane thickness (cm)*)
Di = D0 * Exp[-Edi / (0.001987 * T)];
(* diffusion coefficeint
 for H atoms in Pd (cm^2/s)*)
ßd = ß0 * Exp[-Eb / (0.001987 * T)];
(* rate constant for metal-
```

```
GØ2 = (1 - Ø2)^2;
FØ2 = Ø2;
v02 = ß0 / ((10.154 / (T^0.25)) *
    Sqrt[(GØ2 * Ø2) / (FØ2 * (1 - Ø2)^2)]);
vd2 = v02 * Exp[-Ea / (0.001987 * T)];
P2i = C2i * R * T;
Pm = (P2i + P2) / 2;

FindRoot[
 {J1 == (2 * SØ1 * C1 * (8.3145 * 10^7 * T / (2 * π * M))^0.5) -
    (kd * Ns^2 * z * Ø1 * FØ1 / 2),
  J1 == (Ns * Nb * vd1 * Ø1 * (1 - X1)) -
    (Ns * Nb * X1 * (1 - Ø1) * ßd),
  J1 == Di * Nb * (X1 - X2) / DZ,
  J1 ==
   (Ns * Nb * X2 * (1 - Ø2) * ßd) - (Ns * Nb * vd2 * Ø2 * (1 - X2
  J1 == (kd * Ns^2 * z * Ø2 * FØ2 / 2) -
    (2 * SØ2 * C2i * (8.3145 * 10^7 * T / (2 * π * M))^0.5),
  J1 == 2 * ((Fpk + (Fpv * Pm)) * (C2i * R * T - C2 * R * T))},
 {{Ø1, 0.001, 0 , 10}, {X1, 0.0001, 0 , 10},
  {X2, 0.0001, 0 , 10}, {Ø2, 0.001, 0 , 10},
  {J1, 0, 0 , 10}, {C2i, 0.001, 0 , 10}},
 MaxIterations → 1000]

Y[3] = J1 /. FindRoot[
    {J1 == (2 * SØ1 * C1 * (8.3145 * 10^7 * T / (2 * π * M))^0.5)
      (kd * Ns^2 * z * Ø1 * FØ1 / 2),
     J1 == (Ns * Nb * vd1 * Ø1 * (1 - X1)) -
      (Ns * Nb * X1 * (1 - Ø1) * ßd),
     J1 == Di * Nb * (X1 - X2) / DZ,
     J1 == (Ns * Nb * X2 * (1 - Ø2) * ßd) -
      (Ns * Nb * vd2 * Ø2 * (1 - X2)),
     J1 == (kd * Ns^2 * z * Ø2 * FØ2 / 2) -
```

```
      (2 * SØ2 * C2i * (8.3145 * 10^7 * T / (2 * π * M))^0.5),
    J1 == 2 * ((Fpk + (Fpv * Pm)) *
       (C2i * R * T - C2 * R * T))},
   { {Ø1, 0.001, 0 , 10}, {X1, 0.0001, 0 , 10},
    {X2, 0.0001, 0 , 10}, {Ø2, 0.001, 0 , 10},
    {J1, 0, 0 , 10}, {C2i, 0.001, 0 , 10}},
   MaxIterations → 1000][[5]];

(*STEP4*)
C1 = P14 / (R * T);
Di = D0 * Exp[-Edi / (0.001987 * T)];
ßd = ß0 * Exp[-Eb / (0.001987 * T)];
kd = k0 * Exp[(-2 * Ed) / (0.001987 * T)];
Ø0a = 1 - (2 * Ø1);
SØ1 = S0 * (1 - Ø1)^2;
GØ1 = (1 - Ø1)^2;
FØ1 = Ø1;
v01 = ß0 / ((10.154 / (T^0.25)) *
   Sqrt[(GØ1 * Ø1) / (FØ1 * (1 - Ø1)^2)]);
vd1 = v01 * Exp[-Ea / (0.001987 * T)];
Ø0b = 1 - (2 * Ø2);
SØ2 = S0 * (1 - Ø2)^2;
GØ2 = (1 - Ø2)^2;
FØ2 = Ø2;
v02 = ß0 / ((10.154 / (T^0.25)) *
   Sqrt[(GØ2 * Ø2) / (FØ2 * (1 - Ø2)^2)]);
vd2 = v02 * Exp[-Ea / (0.001987 * T)];
P2i = C2i * R * T;
Pm = (P2i + P2) / 2;

FindRoot[
 {J1 == (2 * SØ1 * C1 * (8.3145 * 10^7 * T / (2 * π * M))^0.5) -
   (kd * Ns^2 * z * Ø1 * FØ1 / 2),
  J1 == (Ns * Nb * vd1 * Ø1 * (1 - X1)) -
   (Ns * Nb * X1 * (1 - Ø1) * ßd),
```

```
 J1 == Di * Nb * (X1 - X2) / DZ,
 J1 ==
  (Ns * Nb * X2 * (1 - Ø2) * ßd) - (Ns * Nb * vd2 * Ø2 * (1 - X2
 J1 == (kd * Ns^2 * z * Ø2 * FØ2 / 2) -
   (2 * SØ2 * C2i * (8.3145 * 10^7 * T / (2 * π * M))^0.5),
 J1 == 2 * ((Fpk + (Fpv * Pm)) * (C2i * R * T - C2 * R * T))},
{ {Ø1, 0.001, 0 , 10}, {X1, 0.0001, 0 , 10},
 {X2, 0.0001, 0 , 10}, {Ø2, 0.001, 0 , 10},
 {J1, 0, 0 , 10}, {C2i, 0.001, 0 , 10}},
MaxIterations → 1000]

Y[4] = J1 /. FindRoot[
   {J1 == (2 * SØ1 * C1 * (8.3145 * 10^7 * T / (2 * π * M))^0.5)
     (kd * Ns^2 * z * Ø1 * FØ1 / 2),
    J1 == (Ns * Nb * vd1 * Ø1 * (1 - X1)) -
     (Ns * Nb * X1 * (1 - Ø1) * ßd),
    J1 == Di * Nb * (X1 - X2) / DZ,
    J1 == (Ns * Nb * X2 * (1 - Ø2) * ßd) -
     (Ns * Nb * vd2 * Ø2 * (1 - X2)),
    J1 == (kd * Ns^2 * z * Ø2 * FØ2 / 2) -
     (2 * SØ2 * C2i * (8.3145 * 10^7 * T / (2 * π * M))^0.5),
    J1 == 2 * ((Fpk + (Fpv * Pm)) *
       (C2i * R * T - C2 * R * T))},
   { {Ø1, 0.001, 0 , 10}, {X1, 0.0001, 0 , 10},
    {X2, 0.0001, 0 , 10}, {Ø2, 0.001, 0 , 10},
    {J1, 0, 0 , 10}, {C2i, 0.001, 0 , 10}},
   MaxIterations → 1000][[5]];

(*STEP 5*)
C1 = P15 / (R * T);
Di = D0 * Exp[-Edi / (0.001987 * T)];
ßd = ß0 * Exp[-Eb / (0.001987 * T)];
kd = k0 * Exp[(-2 * Ed) / (0.001987 * T)];
Ø0a = 1 - (2 * Ø1);
```

```
SØ1 = S0 * (1 - Ø1)^2;
GØ1 = (1 - Ø1)^2;
FØ1 = Ø1;
v01 = ß0 / ((10.154 / (T^0.25)) *
    Sqrt[(GØ1 * Ø1) / (FØ1 * (1 - Ø1)^2)]);
vd1 = v01 * Exp[-Ea / (0.001987 * T)];
Ø0b = 1 - (2 * Ø2);
SØ2 = S0 * (1 - Ø2)^2;
GØ2 = (1 - Ø2)^2;
FØ2 = Ø2;
v02 = ß0 / ((10.154 / (T^0.25)) *
    Sqrt[(GØ2 * Ø2) / (FØ2 * (1 - Ø2)^2)]);
vd2 = v02 * Exp[-Ea / (0.001987 * T)];
P2i = C2i * R * T;
Pm = (P2i + P2) / 2;

FindRoot[
 {J1 == (2 * SØ1 * C1 * (8.3145 * 10^7 * T / (2 * π * M))^0.5) -
    (kd * Ns^2 * z * Ø1 * FØ1 / 2),
  J1 == (Ns * Nb * vd1 * Ø1 * (1 - X1)) -
    (Ns * Nb * X1 * (1 - Ø1) * ßd),
  J1 == Di * Nb * (X1 - X2) / DZ,
  J1 ==
   (Ns * Nb * X2 * (1 - Ø2) * ßd) - (Ns * Nb * vd2 * Ø2 * (1 - X2
  J1 == (kd * Ns^2 * z * Ø2 * FØ2 / 2) -
    (2 * SØ2 * C2i * (8.3145 * 10^7 * T / (2 * π * M))^0.5),
  J1 == 2 * ((Fpk + (Fpv * Pm)) * (C2i * R * T - C2 * R * T))},
 { {Ø1, 0.001, 0 , 10}, {X1, 0.0001, 0 , 10},
  {X2, 0.0001, 0 , 10}, {Ø2, 0.001, 0 , 10},
  {J1, 0, 0 , 10}, {C2i, 0.001, 0 , 10}},
 MaxIterations → 1000]

Y[5] = J1 /. FindRoot[
```

```
{J1 == (2 * SØ1 * C1 * (8.3145 * 10^7 * T / (2 * π * M))^0.5)
   (kd * Ns^2 * z * Ø1 * FØ1 / 2),
  J1 == (Ns * Nb * vd1 * Ø1 * (1 - X1)) -
   (Ns * Nb * X1 * (1 - Ø1) * ßd),
  J1 == Di * Nb * (X1 - X2) / DZ,
  J1 == (Ns * Nb * X2 * (1 - Ø2) * ßd) -
   (Ns * Nb * vd2 * Ø2 * (1 - X2)),
  J1 == (kd * Ns^2 * z * Ø2 * FØ2 / 2) -
   (2 * SØ2 * C2i * (8.3145 * 10^7 * T / (2 * π * M))^0.5),
  J1 == 2 * ((Fpk + (Fpv * Pm)) *
     (C2i * R * T - C2 * R * T))},
 { {Ø1, 0.001, 0 , 10}, {X1, 0.0001, 0 , 10},
  {X2, 0.0001, 0 , 10}, {Ø2, 0.001, 0 , 10},
  {J1, 0, 0 , 10}, {C2i, 0.001, 0 , 10}},
 MaxIterations → 1000][[5]];

(*STEP 6*)
P1[1] := 1.850607493
P1[2] := 2.821064187
P1[3] := 2.395280213
P1[4] := 3.324957416
P1[5] := 3.819561877
(*EXPERIMENTAL RESULTS*)
Ye[1] := 3.58144376 * 10^-6
Ye[2] := 5.57726 * 10^-6
Ye[3] := 4.17163 * 10^-6
Ye[4] := 5.5392417 * 10^-6
Ye[5] := 7.148177 * 10^-6
Table[{Y[i] / 2, P1[i]}, {i, 5}];
<< Graphics`MultipleListPlot`

list1 = Table[{P1[i], Y[i] / 2}, {i, 1, 5}];
list2 = Table[{P1[i], Ye[i]}, {i, 1, 5}];
MultipleListPlot[list1, list2,
 PlotStyle → {Dashing[{Dash}], Dashing[{Dot}]},
 SymbolShape → {PlotSymbol[Star, Filled → True],
```

```
  PlotSymbol[Box]},
 SymbolStyle → {GrayLevel[0], GrayLevel[0.2]}]

(*OPTIMISATION*)

ø = Sum_{i=1}^{5} (Ye[i] - Y[i])^2
```

{Ø1 → 0.700978, X1 → 0.0118751, X2 → 0.00927714,
 Ø2 → 0.646214, J1 → 5.30866×10^{-6}, C2i → 0.0000158012}

{Ø1 → 0.743216, X1 → 0.0146209, X2 → 0.00961218,
 Ø2 → 0.654359, J1 → 0.0000102349, C2i → 0.0000169743}

{Ø1 → 0.727296, X1 → 0.013488, X2 → 0.00947547,
 Ø2 → 0.65108, J1 → 8.19916×10^{-6}, C2i → 0.0000164904}

{Ø1 → 0.758582, X1 → 0.0158532, X2 → 0.00975856,
 Ø2 → 0.657802, J1 → 0.0000124538, C2i → 0.0000175002}

{Ø1 → 0.771052, X1 → 0.0169721, X2 → 0.00988945,
 Ø2 → 0.660824, J1 → 0.0000144727, C2i → 0.0000179774}

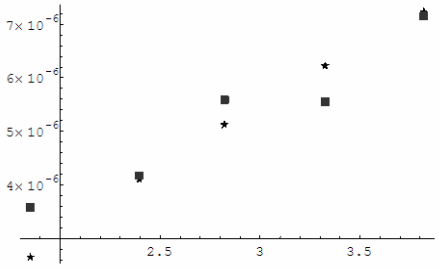

- Graphics -

1.42356×10^{-10}

I2-Program for Model Validation


```
(*Program for model validation*)
P1 = 1;
M = 2.016;
T = 400;
R = 82.0578;
C1 = P1 / (R * T);
P2 = 0;
C2 = P2 / (R * T);
Ed = 10;
Ea = 13.3;
Eb = 5.3;
Edi = 5.3;
k0 = 4.8 * 10^21;
ß0 = 6.8 * 10^13;
D0 = 2.9 * 10^-3;
Nb = 0.113;
Ns = 2.8 * 10^-9;
S0 = 1;
DZ = 10^-4;
Di = D0 * Exp[-Edi / (0.001987 * T)];
ßd = ß0 * Exp[-Eb / (0.001987 * T)];
kd = k0 * Exp[(-2 * Ed) / (0.001987 * T)];
SØ1 = S0 * (1 - Ø1)^2;
v01 = ß0 / (10.154 / (T^0.25));
vd1 = v01 * Exp[-Ea / (0.001987 * T)];
SØ2 = S0 * (1 - Ø2)^2;
v02 = ß0 / (10.154 / (T^0.25));
vd2 = v02 * Exp[-Ea / (0.001987 * T)];
FindRoot[
 {J1 == (2 * SØ1 * C1 * (8.3145 * 10^7 * T / (2 * π * M))^0.5) -
    (kd * Ns^2 * 4 * Ø1 * Ø1 / 2),
  J1 == (Ns * Nb * vd1 * Ø1 * (1 - X1)) -
    (Ns * Nb * X1 * (1 - Ø1) * ßd),
  J1 == Di * Nb * (X1 - X2) / DZ,
  J1 == (Ns * Nb * X2 * (1 - Ø2) * ßd) -
    (Ns * Nb * vd2 * Ø2 * (1 - X2)),
```

```
J1 == (kd * Ns^2 * z * Ø2 * Ø2 / 2) -
  (2 * SØ2 * C2 * (8.3145 * 10^7 * T / (2 * π * M))^0.5)},
{ {Ø1, 0.001, 0 , 10}, {X1, 0.0001, 0 , 10},
 {X2, 0.0001, 0 , 10}, {Ø2, 0.001, 0 , 10},
 {J1, 0, 0 , 1}}, MaxIterations → 1000]
```

Out[300]=

```
{Ø1 → 0.999247, X1 → 0.0241954, 0.00924113 → 0.0239826, Ø2 → 0.999237, J1 → 8.86192×10^-7}
```

I3-Program for Diffusion Limited Flux


```
In[1]:= (*PROGRAM FOR DIFFUSION LIMITED FLUX*)
        (*INPUT VARIABLES*)
        P11 = 1.850607493;
        (*hydrogen gas partial pressure
          in the feed side (atm)*)
        P12 = 2.821064187;   (*hydrogen gas partial
          pressure in the feed side (atm)*)
        P13 = 2.395280213;    (*hydrogen gas
          partial pressure in the feed side (atm)*)
        P14 = 3.324957416;   (*hydrogen gas partial
          pressure in the feed side (atm)*)
        P15 = 3.819561877;    (*hydrogen gas
          partial pressure in the feed side (atm)*)
        P2 = 1.033;          (*hydrogen gas partial
          pressure in the permeate side (atm)*)
        T = 866.483;         (*reactor temperature*)

        M = 2.016;
        Nb = 0.113;
        Ns = 2.8 * 10^-9;
        DZ = 77 * 10^-4;
        D0 = 3.3 * 10^-3;
        Edi = 5.45;
        Di = D0 * Exp[-Edi / (0.001987 * T)];
        Ks = 351.6 * Exp[-1007 / T];
        X11 = P11^0.5 / Ks;
        X2 = P2^0.5 / Ks;
```

```
X12 = P12^0.5 / Ks;
X13 = P13^0.5 / Ks;
X14 = P14^0.5 / Ks;
X15 = P15^0.5 / Ks;

J11 = Di * Nb * (X11 - X2) / (DZ * 2)
J12 = Di * Nb * (X12 - X2) / (DZ * 2)
J13 = Di * Nb * (X13 - X2) / (DZ * 2)
J14 = Di * Nb * (X14 - X2) / (DZ * 2)
J15 = Di * Nb * (X15 - X2) / (DZ * 2)
```

Out[15]= 3.19568×10^{-6}

Out[16]= 6.16123×10^{-6}

Out[17]= 4.93562×10^{-6}

Out[18]= 7.49749×10^{-6}

Out[19]= 8.71372×10^{-6}

Appendix II-Experimental Data for Palladium Membrane (taken from reference 9)

Table 8 Permeate side experimental data for Pd membrane

Run #	Peak Areas					$T_{Reactor}$ (°F)	$P_{Reactor}$ (psi)	Time for 20 cc of gas to flow	
	H_2	N_2	CH_4	CO	CO_2			t_1(s)	t_2(s)
1	2003.94	1519.30	20.06	0.00	8.42	700	40	4.87	4.97
2	5585.96	1050.51	77.00	52.10	92.66	1100	40	4.65	4.6
3	5644.60	1056.14	75.02	51.22	94.72	1100	60	3.6	3.58
4	7055.79	860.20	111.21	65.91	134.57	1100	80	3.71	3.58
5	6727.69	885.17	133.26	93.93	105.69	900	80	4.72	4.43
6	983.00	1587.80	8.01	0.00	0.00	900	60	3.42	3.51
7	1796.05	1510.69	17.89	2.73	3.79	900	40	4.87	4.91
8	1411.51	1555.90	13.90	0.00	1.32	1300	40	3.31	3.18
9	951.20	1624.71	3.00	0.00	1.26	1300	60	3.52	3.6
10	2860.80	1468.98	25.55	14.38	7.85	1300	80	4.68	4.59
11	4113.24	1202.54	62.27	46.01	42.55	900	40	4.8	4.2
12	4105.13	1184.04	81.21	55.77	50.92	900	60	4.13	4.06
13	9180.29	513.11	227.25	200.68	143.24	900	80	3.45	3.41
14	5974.74	1003.42	90.19	96.18	43.03	1300	40	3.74	3.84
15	4747.97	835.02	204.66	186.36	109.27	1300	60	3.65	3.61
16	1402.48	1544.23	8.28	2.53	4.77	1100	40	6.83	7.93
17	1810.87	1442.37	22.27	8.87	14.99	1100	60	4.02	7.82
18	1660.07	1524.33	12.61	6.99	15.20	1100	80	4.41	6.28

Table 9 Feed side experimental data for Pd membrane

Run#	Peak Areas				$T_{Reactor}$(°F)	$P_{Reactor}$(psi)
	H_2	CH_4	CO	CO_2		
1	12152.29	156.83	154.97	288.16	700	40
2	12427.81	197.79	166.13	281.24	1100	40
3	12359.81	186.87	155.94	263.87	1100	60
4	12355.65	190.34	156.98	269.41	1100	80
5	11951.30	233.77	212.74	219.30	900	80
6	11527.71	180.17	174.63	185.22	900	60
7	11349.18	164.23	214.03	194.85	900	40
8	11099.96	168.38	255.99	155.33	1300	40
9	12034.96	154.35	214.93	133.77	1300	60
10	12302.24	179.27	230.24	141.94	1300	80
11	12626.82	228.55	226.83	181.04	900	40
12	11636.09	273.77	237.21	206.01	900	60
13	11458.11	308.38	237.56	219.52	900	80
14	12632.88	211.99	253.45	148.34	1300	40
15	11870.25	228.48	302.34	179.74	1300	60
16	12765.14	276.36	195.85	227.72	1100	40
17	12218.41	289.61	171.89	240.36	1100	60
18	12542.92	268.91	160.11	230.60	1100	80

Table 10 Experimental data for permeate side calibration gases for Pd membrane

Run#	Peak Areas				
	H_2	N_2	CH_4	CO	CO_2
1	17057.17	1759.171	5765.15	1688.526	1590.015
2	17057.17	1759.171	5765.15	1688.526	1590.015
3	17057.17	1759.171	5765.15	1688.526	1590.015
4	17057.17	1759.171	5765.15	1688.526	1590.015
5	17057.17	1759.171	5765.15	1688.526	1590.015
6	17057.17	1759.171	5765.15	1688.526	1590.015
7	17057.17	1759.171	5765.15	1688.526	1590.015
8	17057.17	1759.171	5765.15	1688.526	1590.015
9	17057.17	1759.171	5765.15	1688.526	1590.015
10	17057.17	1759.171	5765.15	1688.526	1590.015
11	16785.72	1670.388	6218.83	1682.023	1562.031
12	16785.72	1670.388	6218.83	1682.023	1562.031
13	16785.72	1670.388	6218.83	1682.023	1562.031
14	16785.72	1670.388	6218.83	1682.023	1562.031
15	16785.72	1670.388	6218.83	1682.023	1562.031
16	17785.78	1577.338	5983.12	1724.646	1506.451
17	17785.78	1577.338	5983.12	1724.646	1506.451
18	17785.78	1577.338	5983.12	1724.646	1506.451

Table 11 Experimental data for feed side calibration gases for Pd membrane

Run#	Peak Areas				
	H_2	N_2	CH_4	CO	CO_2
1	17057.17	1759	5765.15	1688.526	1590.015
2	17057.17	1759	5765.15	1688.526	1590.015
3	17057.17	1759	5765.15	1688.526	1590.015
4	17057.17	1759	5765.15	1688.526	1590.015
5	17057.17	1759	5765.15	1688.526	1590.015
6	17057.17	1759	5765.15	1688.526	1590.015
7	17057.17	1759	5765.15	1688.526	1590.015
8	17057.17	1759	5765.15	1688.526	1590.015
9	17057.17	1759	5765.15	1688.526	1590.015
10	17057.17	1759	5765.15	1688.526	1590.015
11	16785.72	1670	6218.83	1682.023	1562.031
12	16785.72	1670	6218.83	1682.023	1562.031
13	16785.72	1670	6218.83	1682.023	1562.031
14	16785.72	1670	6218.83	1682.023	1562.031
15	16785.72	1670	6218.83	1682.023	1562.031
16	17785.78	1577	5983.12	1724.646	1506.451
17	17785.78	1577	5983.12	1724.646	1506.451
18	17785.78	1577	5983.12	1724.646	1506.451

VITA

Ifeyinwa Jane Iwuchukwu was born in Kaduna, Nigeria on June 20, 1979 to Joseph and Bridget Oranugo. She graduated from the Enugu State University of Science and Technology, Nigeria, with First Class Honors in Chemical Engineering, in December, 2000. From January 2002 to December 2002, she worked as an Assistant Program Supervisor at the Nigerian National Petroleum Corporation, Nigeria. In May 2004 she joined the University of Tennessee Space Institute as a Graduate Research Assistant to pursue a Master of Science degree in Chemical Engineering. She is married to Ernest Iwuchukwu and they have a daughter, Oge Patricia Iwuchukwu.

She plans to join the University of Tennessee, Knoxville, in the fall 2006 to pursue her PhD in Chemical Engineering.